The Journal of Experimental Biology 208, 1125-1146
Published by The Company of Biologists 2005
doi:10.1242/jeb.01507

Jet flow in steadily swimming adult squid

Erik J. Anderson and Mark A. Grosenbaugh*

Department of Applied Ocean Physics and Engineering, Woods Hole Oceanographic Institution, Woods Hole, Massachusetts 02543, USA

*Author for correspondence (e-mail: mgrosenbaugh@whoi.edu)

Accepted 24 January 2005

Summary

Although various hydrodynamic models have been used in past analyses of squid jet propulsion, no previous investigations have definitively determined the fluid structure of the jets of steadily swimming squid. In addition, few accurate measurements of jet velocity and other jet parameters in squid have been reported. We used digital particle imaging velocimetry (DPIV) to visualize the jet flow of adult long-finned squid *Loligo pealei* (mantle length, L_m=27.1±3.0 cm, mean ± S.D.) swimming in a flume over a wide range of speeds (10.1–59.3 cm s^{-1}, i.e. 0.33–2.06 L_m s^{-1}). Qualitatively, squid jets were periodic, steady, and prolonged emissions of fluid that exhibited an elongated core of high speed flow. The development of a leading vortex ring common to jets emitted from pipes into still water often appeared to be diminished and delayed. We were able to mimic this effect in jets produced by a piston and pipe arrangement aligned with a uniform background flow. As in continuous jets, squid jets showed evidence of the growth of instability waves in the jet shear layer followed by the breakup of the jet into packets of vorticity of varying degrees of coherence. These ranged from apparent chains of short-lived vortex rings to turbulent plumes. There was some evidence of the complete roll-up of a handful of shorter jets into single vortex rings, but steady propulsion by individual vortex ring puffs was never observed. Quantitatively, the length of the jet structure in the visualized field of view, L_j, was observed to be 7.2–25.6 cm, and jet plug lengths, L, were estimated to be 4.4–49.4 cm using average jet velocity and jet period. These lengths and an average jet orifice diameter, D, of 0.8 cm were used to calculate the ratios L_j/D and L/D, which ranged from 9.0 to 32.0 and 5.5 to 61.8, respectively. Jets emitted from pipes in the presence of a background flow suggested that the ratio between the background flow velocity and the jet velocity was more important than L/D to predict jet structure. Average jet velocities in steadily swimming squid ranged from 19.9 to 85.8 cm s^{-1} (0.90–2.98 L_m s^{-1}) and were always greater in magnitude than swimming speed. Maximum instantaneous fluid speeds within squid jets ranged from 25.6 to 136.4 cm s^{-1}. Average jet thrust determined both from jet velocity and from three-dimensional approximations of momentum change in successive jet visualizations showed some differences and ranged from 0.009 to 0.045 N over the range of swimming speeds observed. The fraction by which the average jet velocity exceeded the swimming speed, or 'slip', decreased with increasing swimming speed, which reveals higher jet propulsive efficiency at higher swimming speeds. Jet angle, subtended from the horizontal, decreased from approximately 29° to 7° with increasing swimming speed. Jet frequency ranged from 0.6 to 1.3 Hz in the majority of swimming sequences, and the data suggest higher frequencies at the lowest and highest speeds. Jet velocity, angle, period and frequency exhibited increased variability at speeds between 0.6 and 1.4 L_m s^{-1}. This suggests that at medium speeds squid enjoy an increased flexibility in the locomotive strategies they use to control their dynamic balance.

Key words: swimming, squid, *Loligo pealei*, jet propulsion, hydrodynamics, DPIV.

Introduction

Adult *Loligo pealei* and most other squids propel themselves by a combination of fin and jet propulsion (Fig. 1). The relative contribution of the two propulsion systems in many species of squid, including *L. pealei*, varies with swimming speed (Williamson, 1965; Lighthill, 1969; Hoar et al., 1994; Anderson and DeMont, 2005). At low speeds and in hovering, *L. pealei* use both fin and jet propulsion. As swimming speed increases, the contribution of the fins to the production of thrust decreases, fin gait changes, and squid rely more heavily on jet propulsion. At high speeds the fins are often wrapped tightly against the mantle (Williamson, 1965). Squid attain some of their most dramatic speeds and accelerations during escape responses, known as escape jetting (Gosline and DeMont, 1985). During such movements squid rely almost entirely on jet propulsion. In addition to its role in thrust production, the jet is the primary exhalant pathway for respiration (Gosline et

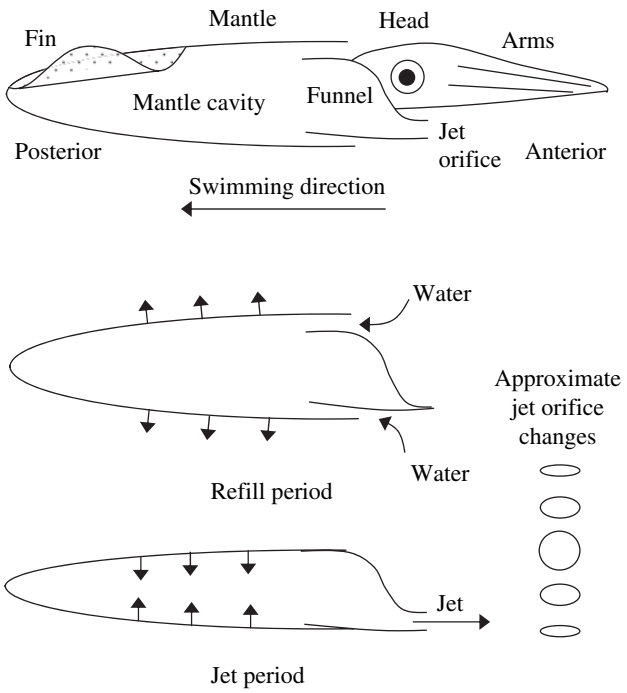

Fig. 1. Sketch of the structures and propulsive mechanisms of the long-finned squid, *L. pealei*. The approximate change in jet orifice shape during jetting is shown.

al., 1983). In this paper, we focus on characteristics of the squid jet in steady swimming.

For more than 40 years, two conflicting models have been used to analyze the hydrodynamics of squid jet propulsion: the 'squirt', or prolonged jet model (Trueman and Packard, 1968; Johnson et al., 1972; O'Dor, 1988; Anderson, 1998; Anderson and DeMont, 2000), and the 'puff', or vortex ring model (Seikmann, 1963; Weihs, 1977). The prolonged jet model assumes the jet to be an elongated mass of high speed fluid. In a real fluid, such jets are marked by a three-dimensional shear layer, through which fluid velocities vary continuously from the velocity of the jet core to that of the surrounding fluid. The shear layer is unstable, which leads to the growth of waves. These waves are the seed points for short-lived vortices whose energy is eventually dissipated into the surrounding flow (Pai, 1954; Drazin and Reid, 1981; Van Dyke, 1982). The rate and character of these developments is dependent upon jet velocity, orifice diameter, fluid viscosity, density and local perturbations in the flow. By contrast, vortex ring propulsion is characterized by the periodic shedding of individual torroidal fluid structures at the trailing edge of the jet nozzle. These torroidal flows, or vortex rings, appear in cross-section as two counter-rotating vortices. Flow at the center of an emitted vortex ring is in the direction of the original emission of fluid from the jet nozzle, unless some other forcing causes the ring to rotate on one of its radial axes. Weihs (1977) demonstrated the availability of impressive hydrodynamic benefits in properly tuned periodic jet propulsion by vortex rings. Nevertheless, the actual fluid structure and velocities in the jets of steadily swimming adult squid have remained largely unknown.

Recently, Anderson (1998), Anderson and DeMont (2000), and Anderson et al. (2001c) performed both quasi-steady and unsteady analyses of squid hydrodynamics using highly accurate kinematic data and whole-body deformation extracted from high-resolution, high-speed video records. Their data revealed that steadily swimming adult *L. pealei* emit relatively large volumes of fluid from a small opening, suggesting the prolonged jet model. At the same time, works focusing on the hydrodynamics of vortex ring formation (Gharib et al., 1998; Linden and Turner, 2001), theorized that jet-propelled organisms, including squid (Linden and Turner, 2001), might use vortex ring propulsion to enhance efficiency. Gharib et al. (1998) observed that the formation of vortex rings in jets emitted from cylindrical pipes into still water was dependent upon the ratio of the length of the plug of fluid expelled from the pipe, L, and the inside diameter of the pipe, D. They found that a solitary vortex ring was formed when $L/D \leqslant 3.6$–4.5. Fig. 2A shows a vorticity contour plot from our experimental repetition of this result (L/D=4.3). Gharib et al. (1998) observed that all the vorticity shed from the pipe was bound up in this single vortex ring and that no other flow structure was present (Fig. 2A). When L/D was greater than about 3.6–4.5 the vorticity shed from the pipe no longer rolled up completely into a single vortex ring. Rather, a leading ring formed and a trail of vorticity followed behind. Fig. 2B shows our repetition of this result for the case of L/D=16. Linden and Turner (2001) used theoretical arguments to arrive at a similar conclusion regarding vortex ring production and the ratio L/D. Most significantly, their analysis predicts that vortex rings produced using the highest possible L/D ratio for the formation of a solitary vortex ring are characterized by the highest ratio of thrust to jet plug kinetic energy. This suggests highest propulsive efficiency. In addition, Krueger and Gharib (2003) showed that vortex rings exhibit a higher average thrust than that predicted by jet plug momentum and attributed the phenomenon to an increase in local pressure above ambient (so-called 'over-pressure'), at the jet orifice, due to the formation of the vortex ring. Even before these findings, Gharib et al. (1998) suggested that '*the mere existence of the formation number…hints at the possibility that nature uses this time scale…*', e.g. in propulsion.

Preliminary investigations of jet volume flow and wake structure in steadily swimming adult squid, however, have not suggested that their locomotive structure and behavior take advantage of the potential benefits of L/D ratios near 4. On the contrary, Anderson et al. (2001a) reported L/D ratios as large as 40 in steadily swimming adult *L. pealei*. Furthermore, the data of Anderson (1998) and Anderson and DeMont (2000) can be used to determine L/D ratios of 39.2–67.2, also in steadily swimming *L. pealei*. Bartol et al. (2001b) reported L/D ratios of 3–17 in small *L. brevis* (L_m<3.0 cm) and 10–40 in large and intermediate-sized individuals. They claim that benefits from periodic vortex ring propulsion as described by Weihs (1977) might be obtained in smaller squid. Jets visualized by dye injection from two small squid (mean L_m=4.2 cm) swimming more or less steadily were reported to have left several vortex

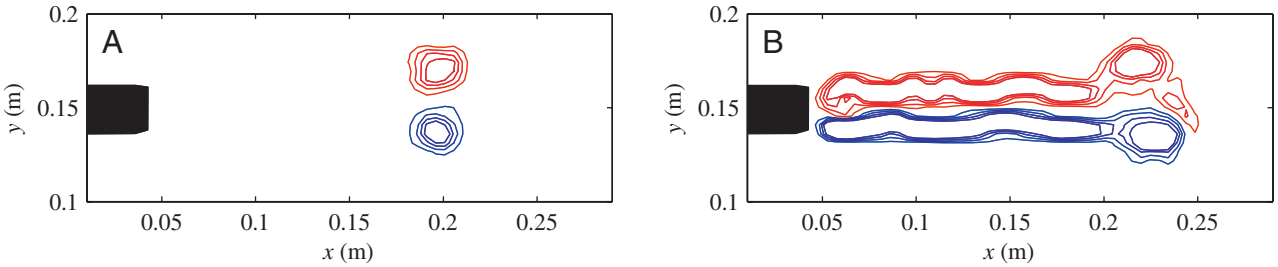

Fig. 2. Vorticity contour plots for jets emitted from a pipe with a sharp trailing edge into still water. (A) L/D=4.3, t=6.7 s, $t/\Delta t_j$=3.4, and (B) L/D=16, t=6.7 s, $t/\Delta t_j$=0.8, where L is the piston stroke length and D is the pipe inside diameter (2.39 cm). Piston velocity, u_p=5.0 cm s^{-1}. Red contours represent counterclockwise, or positive, vorticity and blue contours represent clockwise vorticity. Contour magnitudes are 0.5, 1.0, 1.5 and 2.0 rad s^{-1}. Magnitude increases monotonically from the outermost (0.5 rad s^{-1}) contour to the interior of any jet structure. Note that in B the closing of contours near the jet nozzle is an artifact of DPIV. In reality, these contours originate on the inner and outer surfaces of the pipe from which the jet is emitted.

rings in the wake (Bartol et al., 2001b). Some highly turbulent jets were emitted from these squid with no vortex rings present, but this occurred when the squid swam erratically, apparently in response to irritation caused by dye injection. In addition, Bartol et al. (2001b) hypothesize that larger squid, '*…probably produce vortex rings that are too widely spaced to benefit significantly from ring interaction*.' Although our data do not suggest that adult *L. pealei* use periodic vortex ring propulsion, jet frequencies and swimming speeds from Anderson and DeMont (2000) and the present work similarly predict wide spacing (>40 cm) between sequentially emitted jet structures in adult *L. pealei*.

Despite such observations and predictions about squid jet structure relative to the ratio L/D, the pipe experiments of Gharib et al. (1998), from which the importance of the ratio was revealed, differ in a significant way from jetting in swimming squid: they were conducted in still water. By contrast, the jets of squid issue into a background flow past the jet nozzle due to the motion of the squid through the water. Thus, the question arises as to whether or not a simple L/D ratio is sufficient to predict squid jet structure. The significance of this background flow and the failure of L/D ratios from experiments in still water to predict structure in this case were pointed out by Anderson et al. (2001a) in a preliminary analysis using the squid and pipe jet data presented here. They reported that vorticity shed into the wake from the outer boundary layer apparently contributed to a change in jet structure. The sign of the outer boundary layer vorticity is opposite to that of the jet vorticity, and its magnitude is dependent on swimming speed, body shape and angle of attack. Consider the extreme case when background flow velocity is greater than jet velocity. Intuitively, one realizes that a vortex ring, such as in Fig. 2A might never form, regardless of L/D, since the outer boundary layer vorticity would likely dominate the downstream flow development. In response to this finding, Jiang and Grosenbaugh (2002) numerically simulated jets from pipes in the presence of background flow and confirmed the significance of background flow on jet structure, as observed in our squid and pipe jet experiments. Specifically, Jiang and Grosenbaugh (2002) report a decrease in the L/D ratio necessary to produce a single vortex ring puff as background flow is increased. Work by Krueger et al. (2002, 2003) independently confirmed this finding, with some slight differences due to their use of different initial conditions.

In this paper, we present the results of flow visualization from (1) a large number of jets emitted from steadily swimming adult squid, and (2) pipe jet experiments with a background flow parallel to the jet. For squid, we use flow field data to investigate not only jet structure, but also trends in parameters such as jet velocity, slip, jet frequency, jet angle, thrust and propulsive efficiency as functions of swimming speed.

Materials and methods

Animals

Long-finned squid *Loligo pealei* Lesueur (N=6) were caught with squid jigs or by trawl in Nantucket Sound and Woods Hole, MA, USA. The animals were kept in 750-liter holding tanks with a constant flow of seawater from Nantucket Sound and were fed baitfish common to that region. Squid were transferred to and from their tanks in 30-liter buckets or 60-liter coolers. All experiments were conducted within 1–4 days of capture. Following the experiments, squid were euthanized by decapitation with a sharp blade. Body length of the squid, L_s, ranged from 32 to 39 cm (36.3±3.1 cm, mean ± S.D.). Mantle length L_m ranged from 22.2 to 30.2 cm (27.1±3.0 cm, mean ± S.D.). Wet mass ranged from 224 to 369 g (281±52 g, mean ± S.D.).

Swimming conditions

A total of 116 squid jets were recorded in 42 swimming sequences in which squid were holding station in the flow. The number of consecutive jets per sequence ranged from 1 to 14. The squid swam in a test section 80 cm long and 23 cm deep. The width of the test section was varied when necessary to increase the time spent by the squid in the plane of the laser sheet that was used to illuminate the flow. Three different test section widths were used: 15 cm (86 jets), 35 cm (25 jets) and 40 cm (5 jets). The test section was constructed in a large,

recirculating, open-channel flume (30 cm deep and 78 cm wide) capable of speeds up to 62 cm s^{-1} and temperature control to within ±0.1°C. Flow speeds, U, in the test section were determined from the same DPIV records that were used for jet analysis and ranged from 10.1 to 59.3 cm s^{-1}, i.e. 0.33 to 2.06 L_m s^{-1}. Water temperature in the flume and holding tanks ranged from 12.5 to 19.5°C, corresponding to daily temperatures in the waters of Nantucket Sound. A honeycomb flow-through barrier was placed at the upstream end of the test section to damp out large-scale flow disturbances. The barrier was 12.7 cm in streamwise length with a tube diameter of 1.3 cm. A plastic grid bound the downstream end of the test section (grid size, 1.5 cm; bar width, 0.2 cm; streamwise length, 0.8 cm). Laser Doppler anemometry from a previous experiment in the same flume revealed turbulence intensities of 4–6% over the range of experimental flow speeds (Anderson et al., 2001b). These fluctuations in flow velocity are significantly lower than those produced by the presence and jetting of the squid.

Flow visualization

Flow around the swimming squid was visualized by digital particle imaging velocimetry, DPIV (Adrian, 1991; Willert and Gharib, 1991). DPIV uses cross-correlation to determine the average displacement of groups of seeding particles in consecutive stroboscopic images of a two-dimensional slice of a flow field. The particles are grouped in sub-windows of the field of view by a user-defined grid. A pulsed laser sheet is used to illuminate the flow, and is synchronized with a digital video camera so that it flashes once in each video frame. The camera is pointed at right angles to the laser sheet. The velocity field of the flow is determined by dividing average local displacements of seeding particles in the flow by the time step, Δt, between the laser pulses. In this work, we used a hybrid DPIV code that performs a quick FFT estimate of sub-window displacements and then refines the estimate to sub-pixel accuracy by local cross-correlation (McKenna and McGillis, 2002). Sub-windows were 32×32 pixels with an overlap of 16 pixels.

To capture the jets of swimming squid, which are emitted from the ventral side near the trailing end (Fig. 1), we oriented our laser sheet (New Wave Research, Fremont, CA, USA; Nd:YAG) streamwise and vertical by one of two methods: (1) directing the laser sheet up through the transparent bottom of the flume, or (2) deflecting the beam upstream with a thin (3 cm × 40 cm), vertical mirror at an angle of 45° to the flow, submerged at the downstream end of the test section. In the latter arrangement, data was only acquired when the squid trailing edge was >1 body length upstream of the mirror to minimize artifacts caused by its presence in the flow. The two arrangements were used to optimize resolution at different fields of view. A single side-view camera (Megaplus ES 1.0, Roper Scientific, Vianen, The Netherlands; 1008×1018 pixels) was used to visualize fields of view ranging from 25 to 30 cm on a side. The laser sheet was 1–2 mm thick and the flow was seeded with silver-coated, hollow glass spheres, 10 μm in diameter (DANTEC, Skovlunde, Denmark). The time step, Δt, between laser pulses was set at 2–10 ms, depending on swimming speed to optimize particle displacements (McKenna and McGillis, 2002). The laser pulse length, or exposure time, was 3–5 ns with an available power of 500 mJ per pulse. However, power was attenuated significantly to minimized irritation to the animal. The camera was operated at 30 Hz. Therefore, pairs of exposures, or image pairs, were acquired at 15 Hz. Up to 700 sequential images were acquired per swimming sequence.

It should be mentioned here that DPIV has some limitations when calculating flow velocities near bodies, such as squid and pipes. The basic DPIV algorithm, i.e. cross-correlation, is not able to distinguish between particles in a flow and patterns on the surfaces of bodies. If the sub-window being analyzed includes seeded flow and a body surface moving relative to each other, the patterned region with the higher combination of brightness and amount of bright area will dominate the velocity calculation in that region. The deformation of the flow due to shear near the body also affects the velocity calculation since it alters the pattern of the seeding particles. Usually, the algorithm results in a velocity somewhere between that of the body surface and that of the flow. Theoretical and experimental fluid dynamics tell us that there is, indeed, a continuous variation in fluid velocity from zero at the body surface with respect to the body to the background flow velocity at a certain distance from the surface (which is relatively monotonic in the general case). Therefore, although the magnitudes of velocity and vorticity calculated in this shear layer are biased, the sign of the vorticity, and upper-bound values of boundary layer thicknesses, may be trusted. We have certainly not attempted to make any quantitative conclusions from the DPIV data where affected by body surfaces, but vorticity contours and velocities along the squid and pipe surfaces are left in our plots for instructive reasons (e.g. Fig. 3). Due to the resolution used in our experiments velocities at points greater than 0.34 cm away from a body surface and vorticities greater than 1.0 cm away are calculated from sub-windows that do not include the body. An example of a clear artifact due to the presence of a body can be seen in Fig. 2B. Note the closure of the parallel vorticity contours of same sign near the pipe orifice. Fluid theory states that during jetting the vorticity contours actually originate on the surfaces of the pipe and piston. Numerical simulations of pipe jets demonstrate this fact (Jiang and Grosenbaugh, 2002). However, since the pipe is stationary, zero velocities are calculated by DPIV over the majority of the area within the silhouette of the pipe. This results in zero vorticities over much of the same region, and the contour plotting program closes the non-zero jet vorticity contours outside this region of the plot.

Squid jet analysis

The fluid structure of squid jets was analyzed qualitatively using velocity field plots and vorticity contour plots, but we were also able to digitize the region of the jet and extract quantitative information such as jet length, width, angle and

average jet velocities. Preliminary inspection of the video records and velocity fields around swimming squid showed that in every case, average jet velocity was greater than the background velocity. Therefore, the structure of the jet was digitized by taking the region within which flow speeds were at least 5% greater than the maximum background flow speed upstream of the jet and away from the squid. 5% was used because, in general, it appeared to be the lowest threshold that correctly filtered out velocities due to the variation in the flume flow, while correctly digitizing the jet.

Since jet structure was observed to be relatively elongated and straight, with a central core made up of the highest velocity fluid, a jet centerline was determined to aid in the analysis. A rough centerline was drawn manually in MATLAB for each visualization (i.e. each processed image pair) that exhibited a jet flow. The centerline line was refined iteratively by calculating a best-fit line through the centroids of velocity calculated in slices of the jet perpendicular to the previously estimated centerline, starting with the rough centerline. For three-dimensional approximations, we treated the slices as disks. We call the disk diameter, 'the diameter of the jet fluid structure', or more simply, 'jet structure diameter', D_j. Length of the visualized jet fluid structure, L_j, and jet angle, β, were also determined using the jet centerline. Jet angle was determined early in the jet period to avoid artifacts resulting from the deformation of the jet in its later development. A proper jet angle measurement was possible in 110 of the 116 jets. In addition to the centerline, we determined a curve for each jet representing the position of maximum velocity in the slices perpendicular to the refined centerline. In general, this curve followed the centerline closely. We refer to the velocity along this curve as jet core velocity, u_{jc}. The average jet core velocity, $\bar{u}_{jc}$, is defined as the spatial average velocity along this curve.

We calculated average jet velocity in three ways to generate (1) a standard value, $\bar{u}_j$, (2) an upper-bound value, $\bar{u}_{jH}$, and (3) a lower-bound value, $\bar{u}_{jL}$, for each jet. The standard value was calculated by taking the time average of the average jet core velocity, $\bar{u}_{jc}$, during a given jet period. The upper bound was calculated by taking the time average of the maximum jet core velocity. The lower-bound value was calculated by taking the time average of the average jet velocity over the entire jet structure, taken in slices of the jet perpendicular to the centerline. The value for each slice was weighted by slice volume, assuming the slices to be disks of diameter D_j to account roughly for three-dimensionality. Although this is clearly an approximation, it results in a lower estimate than a simple area-based average of the jet cross-section, since slices where D_j was larger tended to have lower velocities. A fully axi-symmetric rendering of the jets was not used for the lower-bound calculation because the jet velocities were not always sufficiently symmetric about the centerline or the jet core curve. The actual average jet velocity is expected to lie somewhere between the standard value, $\bar{u}_j$, and the lower-bound value, $\bar{u}_{jL}$. It should also be noted that our jet velocities have likely been decreased by deceleration and entrainment, especially the lower-bound value, as the jet fluid enters the surrounding fluid. With that in mind, and assuming the jet profile at the jet orifice to be relatively undeveloped due to the short, funnel-shaped nozzle, we use the standard value as the best estimate of actual average jet velocity. Therefore, unless otherwise specified, the term average jet velocity, when used in reference to our data, refers to the standard value, $\bar{u}_j$. The term jet velocity, u_j, will be used here to represent instantaneous jet velocity assuming a constant velocity profile at the jet orifice.

Two measurements of jet length were used to compare the data from all squid jets observed. We call the first 'jet structure length', L_j. It is defined as the maximum length observed for the digitized fluid structure of the jet during the jet period. This measurement frequently underestimated the actual length of the jet structure, because (1) the jets of squid often extended beyond of the field of view and (2) the squid were often slightly 'yawed' during jetting. Yaw is the angle between the oncoming flow and the dorso-ventral plane of the animal. We determined yaw qualitatively from the side-view images, as evidenced by unequal lighting by the laser sheet along the squid body. Yaw resulted in jets that passed through the laser sheet, and the cross-section of a jet thus visualized is almost without exception shorter than the jet itself.

The second measurement of jet length used was 'jet plug length', L, which was determined by multiplying the average jet velocity by the jet period, Δt_j. Upper and lower bounds for L were also determined using the upper and lower-bound average jet velocities. We define jet period here, as the time over which the jet orifice was observed to be fully open as determined from the video records. In general, this period tended to be the majority of the time between orifice opening and closing. Anderson and DeMont (2000) observed the same behavior and included a detailed plot of jet diameter as a function of time. Of the 116 jets that were recorded, the jet nozzle was visible in 89. We report jet structure length L_j and jet plug length L in proportion to the average jet orifice diameter D of 0.8 cm during the jet period, as measured by Anderson and DeMont (2000) on similarly sized *L. pealei.* This allows our squid jet data to be viewed in comparison to the pipe jet experiments of Gharib et al. (1998).

Jet frequency f and average jet frequencies f_{avg} were determined from our video records. The frame numbers of the images in which the jet nozzle first opened were recorded when possible. The number of frames between consecutive jet openings was divided by the frame rate of the camera (30 Hz) to obtain the elapsed time between the jets. This time period is called the 'locomotive period' rather than the 'jet period' because it represents a full locomotive cycle, i.e. jetting and refilling. Locomotive period was then inverted, yielding jet frequency, f. There were 61 full locomotive periods in which the jet nozzle was visible. Jet frequency was calculated for each of the 61 periods. From these 61 values, f_{avg} was determined for each set of all locomotive cycles representing the same squid and swimming speed. Only sets with at least three

locomotive cycles were used. There were 9 such sets spanning the full range of swimming speeds observed.

Propulsive efficiency

Propulsive efficiency is the hydrodynamic efficiency during propulsion. Anderson and DeMont (2000) found that the equation they derived for the hydrodynamic efficiency of squid during jetting was the same equation used in fluid dynamics to determine propulsive efficiency in rockets (Streeter and Wylie, 1985; Houghton and Carpenter, 1993). In addition, they derived an equation for the hydrodynamic efficiency in squid for the whole locomotive cycle. Anderson and DeMont (2000) explain that these two equations are the appropriate efficiency equations for squid, rather than the Froude efficiency equation, since Froude efficiency assumes a constant forward intake of the working fluid while squid use an aft-facing intake system (Fig. 1). In this investigation, we have extended the hydrodynamic efficiency equations prescribed for squid by Anderson and DeMont (2000) to include jet angle. Anderson and DeMont (2000) incorporated jet angle into propulsive efficiency by simply using the axial component of jet velocity for jet velocity, u_j, in their equations. This approach, however, does not correctly account for the decrease in efficiency expected due to a non-zero jet angle.

The derivation of hydrodynamic efficiency, η, begins with the equation,

$$\eta = \text{useful work} / (\text{useful work} + \text{wasted energy}) , \quad (1)$$

Fluid theorists have defined the rate of useful work as thrust T multiplied by forward velocity, thus TU (Prandtl, 1952; Streeter and Wylie, 1985; Houghton and Carpenter, 1993). This is applied both to stationary propellers with flow past and to propellers translating at constant velocity. Wasted energy is defined as any kinetic energy left in the wake as a result of jetting relative to the surrounding flow, that is, the kinetic energy of the jet signature. This is best understood considering an astronaut who is propelled by throwing a wrench *vs* pushing off an immovable object using the same force for the same amount of time. In both cases the astronaut is accelerated to the same speed, but in the former case the astronaut does more work because the wrench gives way, or 'slips'. That is, the force acts over an additional distance. This is analogous to a fluid dynamic concept known as 'slip'. Slip is simply the fraction by which jet velocity exceeds or falls short of the surrounding flow speed and is frequently used as an indicator of propulsive efficiency in an inverse sense. High slip indicates low efficiency. It is defined as $u_j/U–1$, where u_j is the jet velocity, assuming uniform, ideal flow, and U is the velocity of the surrounding fluid, both with respect to the jet orifice. Slip is traditionally defined as one-dimensional, i.e. with u_j and U in the same direction. Nevertheless, it is obvious that a jet issued at an angle β to a uniform flow has greater 'slip' than $u_j/U–1$. If the angle between U and u_j were increased to 90°, slip would be infinite. Therefore one might argue that the definition of slip could be expanded to include a jet angle by substituting the component of U in the direction of u_j for U in the equation of slip, i.e. slip=$u_j/(U\cos\beta)–1$. In this paper, we calculated slip using this equation and the one-dimensional form, for comparison.

If u_j is in the same direction as U, the rate at which excess kinetic energy is added to the surrounding fluid is $\rho Q(u_j–U)^2/2$, where ρ is the jet fluid density, and Q is the rate of volume flow out of the jet. For ideal, uniform jet flow, thrust is $\rho Q u_j$ and therefore the rate of useful work, TU, is $\rho Q u_j U$. Substituting these into Eq. 1, one arrives at the equation for rocket motor propulsive efficiency, η_r:

$$\eta_r = 2Uu_j / (U^2+u_j^2) . \quad (2)$$

If instead we define an angle β between u_j and U, excess kinetic energy becomes $\rho Q[(u_j\cos\beta–U)^2+(u_j\sin\beta)^2]/2$ and useful work becomes $\rho Q(u_j\cos\beta)U$. Substituting these into Eq. 1, we find that the propulsive efficiency of a jet, η_j, issuing at an angle β to U is:

$$\eta_j= 2Uu_j\cos\beta / (U^2+u_j^2) . \quad (3)$$

Since we define jet angle as the angle between u_j and U, any useful work done by the vertical component of the squid jet during the jet period can be incorporated if the vertical motion of the body during jetting is known. U and β can then be determined from the resultant of the horizontal and vertical body velocities. Anderson (1998) observed small upward movements (<1 cm) in steadily swimming adult *L. pealei* during jetting apparently due, in part, to the vertical component of the jet. When these motions are accounted for, TU increases, jet angle decreases and wasted kinetic energy decreases, therefore propulsive efficiency increases. Nevertheless, the contribution is expected to be very small, especially at high swimming speeds, where the horizontal swimming speed dominates the motion of the squid. Anderson (1998) reports a vertical speed of about 1.6 cm s^{-1} during the jet period of a squid swimming with a horizontal speed of 25 cm s^{-1} (1.0 L_m s^{-1}) and a jet angle of 30°. Taking this vertical motion into account, we calculate an increase in propulsive efficiency during the jet period of just 2%.

If we begin again with Eq. 1, treat the work required for mantle refill as wasted energy and assume that the same volume of fluid is taken in as jetted out in any cycle, we obtain the whole-cycle hydrodynamic efficiency for squid, η_{wc}:

$$\eta_{wc}= 2Uu_j\cos\beta / (2u_R U+3U^2+u_j^2) , \quad (4)$$

where u_R is the refill velocity relative to the body at the intake orifice. As in the derivation of the whole-cycle efficiency equation of Anderson and DeMont (2000), the assumption that the total volume emitted during jetting is equal to the total volume taken in during refill results in the convenient elimination of jet period Δt_j and refill period Δt_R from the equation. Once again, a simple multiplier of $\cos\beta$ in the numerator turns out to be the only difference between the corresponding one-dimensional equation derived by Anderson and DeMont (2000). Anderson and DeMont's whole-cycle hydrodynamic efficiency predicts a theoretical

limit of 58%, due largely to the cost of mantle refill. This limit is approached when u_j=1.7U and u_R is small. The same is true for Eq. 4, except that the theoretical limit is 58% × cosβ. Both Eqs. 3 and 4 demonstrate clearly and correctly that propulsive efficiency decreases to 0 as jet angle increases from 0° to 90°.

At the present time, no accurate measurements of refill velocities have been achieved. Mantle refill volume flows have been measured (Anderson and DeMont, 2000), but refill orifice area is unknown. Therefore refill velocities must be estimated to calculate whole-cycle efficiencies. We have estimated the average refill area to be approximately 2–3 times the jet orifice area, based on rough visual estimates. Refill periods Δt_R, in general, are about 1–2 times the jet period Δt_j, based on our data and that of Anderson and DeMont (2000). Therefore, assuming that the average volume outflow during jets is equal to average volume intake during refill in steady swimming, we estimated refill velocities to be 0.17–0.5 times jet velocity and used this range in calculations of whole-cycle propulsive efficiency.

It should be noted here that Eqs. 2 and 3 produce the most accurate values of efficiency when instantaneous values of u_j, U and β are available. An accurate average propulsive efficiency during the jet period can then be determined from the time average of the instantaneous efficiency over the jet period. This is for the simple reason that the time average of u_j^2, for example, is not the same as $\bar{u}_j^2$ unless u_j is constant. The same is true in division, multiplication, cosine and other non-linear mathematical functions. By contrast, it is incorrect to use instantaneous values in Eq. 4 since the equation represents the whole cycle as a unit, therefore time averaged values for u_j, u_R, U and β during their respective periods must be used. If the instantaneous values spend most of the time far below and far above their time averages, it is better to return to first principles (Eq. 1) and rigorously determine efficiency from useful work and wasted kinetic energy. Nevertheless, we and Anderson and DeMont (2000) have observed that steadily swimming adult squid maintain u_j, U and β with relatively small variation about their time averaged values for the majority of their respective periods, and Eqs. 2, 3, and 4 are expected to give meaningful efficiencies even using time averaged values. As a test of Eq. 2, total kinetic energy, KE_T, and excess kinetic energy, KE_e, of the jet fluid were calculated from a three-dimensional approximation of jet velocity from all jet visualizations. These were used to calculate propulsive efficiency by $(KE_T–KE_e)/KE_T$.

Pipe jet experiments

Jets emitted from a cylindrical pipe were visualized using DPIV. Fluid was driven out of the pipe by a motor-actuated piston. The inside and outside diameters of the pipe were 2.39 and 2.54 cm, respectively. The trailing edge of the pipe was beveled to about 30° to form a sharp edge with a diameter equal to the inside diameter, D. The pipe was aligned parallel to the bulk flow in the flume (i.e. streamwise) and centered between the top, bottom and side walls. The free surface was eliminated with a sheet of acrylic. Total water depth was 22 cm and the side walls were 78 cm apart. The pipe was mounted so that the outer flow over the last 1.2 m section of pipe encountered no mounting structures to interrupt the flow. A faired beam coupled the piston to its motor 3 m upstream of the jet nozzle. In general, the piston program consisted of a rapid acceleration, followed by constant speed and a rapid deceleration, similar to the time course of jet velocity u_j observed in *L. pealei* (Anderson and DeMont, 2000). Piston velocities u_p, i.e. average jet velocities, ranging from 1 to 10 cm s^{-1} and background flow speeds U of 0–15 cm s^{-1} were used. Ratios of jet plug length to jet orifice diameter, L/D, ranging from 2 to 16 were examined. Experiments in which jets were emitted into still water (U=0) were performed to show that the apparatus gave results that matched those of Gharib et al. (1998) (Fig. 2).

The purpose of our pipe experiments was to examine the effect of background flow on jet structure and to attempt to mimic the fluid structures observed in the jets of squid. When squid jet, the nozzle opens suddenly on the dorsal side of the body and fluid is emitted at various angles to the horizontal. The jet is emitted into the surrounding flow, not into the wake of the squid, and is affected by a boundary layer that begins peeling off the trailing edge of the jet nozzle the moment it opens. With this in mind, we developed a technique that we call ‘pre-jetting’ for use in our pipe jet experiments. In pre-jetting, we moved the piston at the same speed as the background flow until the flow behind the pipe was much more similar to the background flow than to the wake of the pipe while not jetting. This was determined from preliminary visualizations of the flow. Immediately following pre-jetting, the piston program for the jet was started. We do not assert that our pipe and squid jet initial conditions are identical. Pre-jetting certainly does not eliminate the vorticity shed from the inner and outer boundary layers of the pipe, and therefore the flow into which the jet was emitted was not entirely uniform. Also, the flow past the jet nozzle of the squid is certainly not uniform about the circumference of the nozzle, due to the close proximity of the nozzle to the head and arms (Fig. 1). Nevertheless, in both cases, jets are emitted into a background flow, not a wake, and they are impacted by boundary layers separating from the trailing edge of the jet nozzle. Furthermore, the fluid structure of pipe jets modulated in this way most closely resembled squid jets. Two other initial conditions were attempted in pipe jets: (1) starting the piston from rest and emitting the jet into the wake of the pipe, and (2) sucking the wake into the pipe before jetting. Both situations resulted in vortex patterns that were, in general, qualitatively less similar to those of squid jets. Krueger et al. (2003) used different initial conditions in which both the background flow and the jet flow start from rest. Although this may mimic a jet-propelled organism starting from rest, it is different from the initial conditions for a jet emitted from a steadily swimming squid. Some earlier examples of visualizations of jets in the presence of background flow are displayed by Yamashita et al. (1996).

Results

The jet structure of swimming squid

Visualization of the jets of steadily swimming adult *L. pealei* (Figs 3, 4, 5) revealed two consistent characteristics of jet structure: (1) an elongated shape, and (2) the reduced and/or late development of the leading vortex of the jet compared to jets in still water (Fig. 2B). Propulsion by individual vortex ring puffs shed at the jet nozzle, i.e. pulsed vortex ring propulsion, was never observed in steadily swimming adult squid. These findings were observed in consecutive jets by individual squid swimming at the same swimming speed (Fig. 3), in the jets of different squid swimming at nearly the same speed (Fig. 4), and in the jets of different squid swimming at greatly differing swimming speeds (Fig. 5). In each case, the jets broke up into vortical structures with varying degrees of coherence (Fig. 6). These structures occasionally suggested short-lived chains of vortex rings (Fig. 6A,B), but were usually somewhat less organized (Fig. 6C,D). In most cases, the jet flow was convected downstream, out of the field of view before any evidence of final transition to turbulence

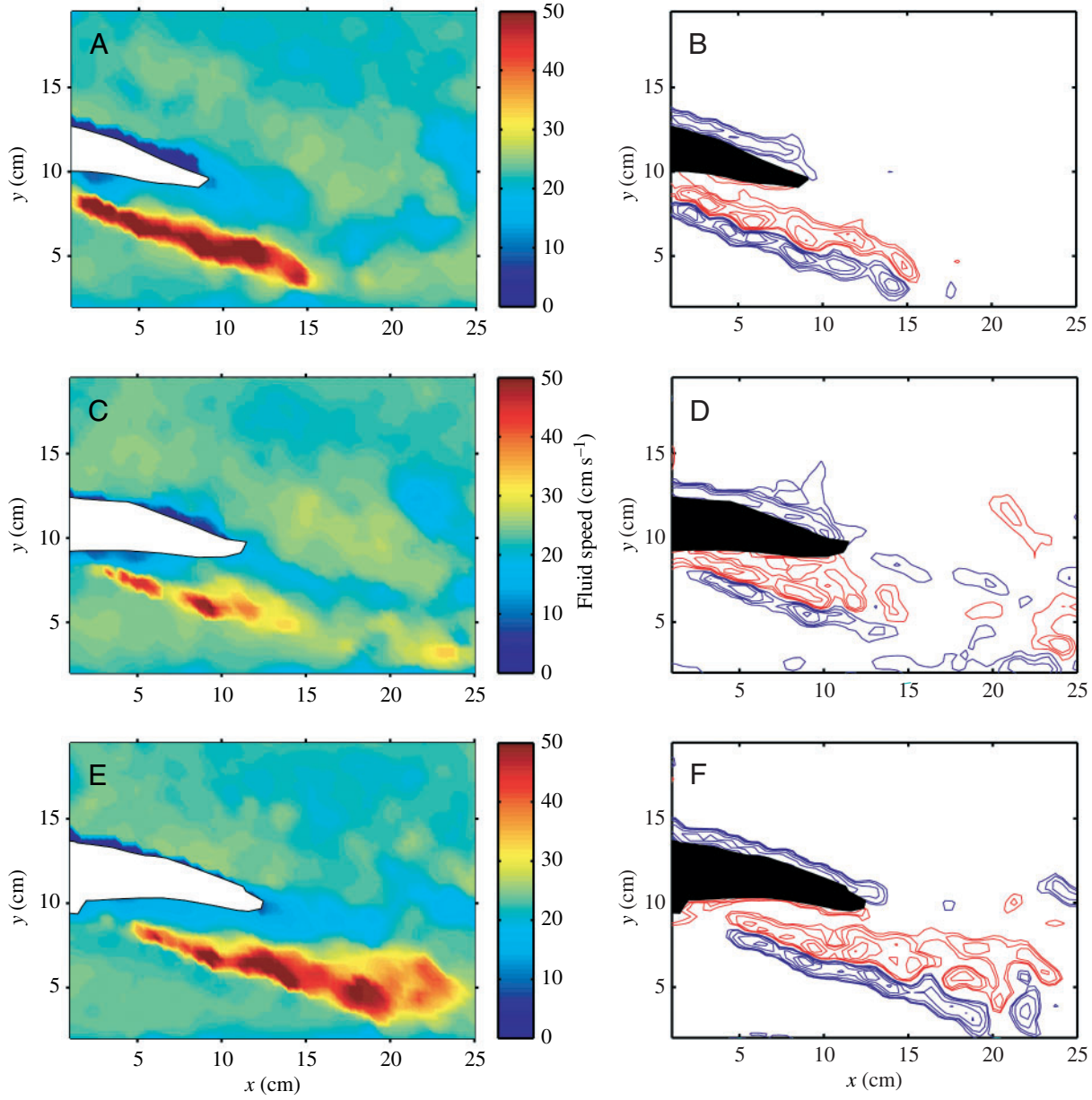

Fig. 3. Velocity magnitude (A,C,E) and vorticity contour plots (B,D,F) during three separate, consecutive jets of an adult *L. pealei* holding position at 25 cm s^{-1}. Flume flow is from left to right. The aft section of the squid is shown in white in the velocity magnitude plots and in black in the corresponding vorticity contour plots. The elongated region of fast moving fluid is the jet. The magnitudes of vorticity contours are (B) 4, 6, 10, 15 and 20 rad s^{-1}, (D) 2, 4, 6, 10, 15 and 20 rad s^{-1}, and (F) 3, 4, 6, 10, 15 and 20 rad s^{-1}. See explanation of contour identification in Fig. 2. These are not consecutive image pair visualizations; rather each set of plots represents the flow at some instant during the jet period of three consecutive jets. (A,B) t=0.3 s, $t/\Delta t_j$=1.0, (C,D) t=0.7 s, $t/\Delta t_j$=1.2, and (E,F) t=0.5 s, $t/\Delta t_j$=0.9.

could be observed. However, such transition was observed in a few cases in which the jet nozzle was close to the upstream edge of the visualization (Fig. 6E,F). In a few of the shorter jets, there was the suggestion of a more complete roll-up of the jet into a vortex ring, but this was the exception to the rule. An interesting effect is displayed in the plots of the highest swimming squid in Fig. 5. The dorsal boundary layer separates dramatically compared to lower speeds, creating a large wake with areas of elevated vorticity, comparable to that in the jet, at the wake boundary. This is a less favorable hydrodynamic condition revealing potentially high pressure drag.

Velocity vectors were left out of Figs 3–6 since the plots were intended to demonstrate the basic structure of the jet. Furthermore, the jet velocity was generally parallel to the axis of the elongated jet structure. A representative jet is shown in more detail and with vectors in Figs 7 and 8. Fig. 7A shows the velocity field from Fig. 3A at a higher resolution and with velocity vectors. Even at this resolution every other vector has been removed for clarity. The jet itself, extracted, rotated to the horizontal, and enlarged is shown in Fig. 7B. Fig. 8A shows the same point of view, but with the freestream velocity subtracted out. There is some evidence of weak circuitous flow in a few regions and possibly a weak vortex ring near the leading end of the jet. In order to best identify vortices visually, one must subtract the velocity of each potential vortex center. This treatment confirmed the development of weak vortical

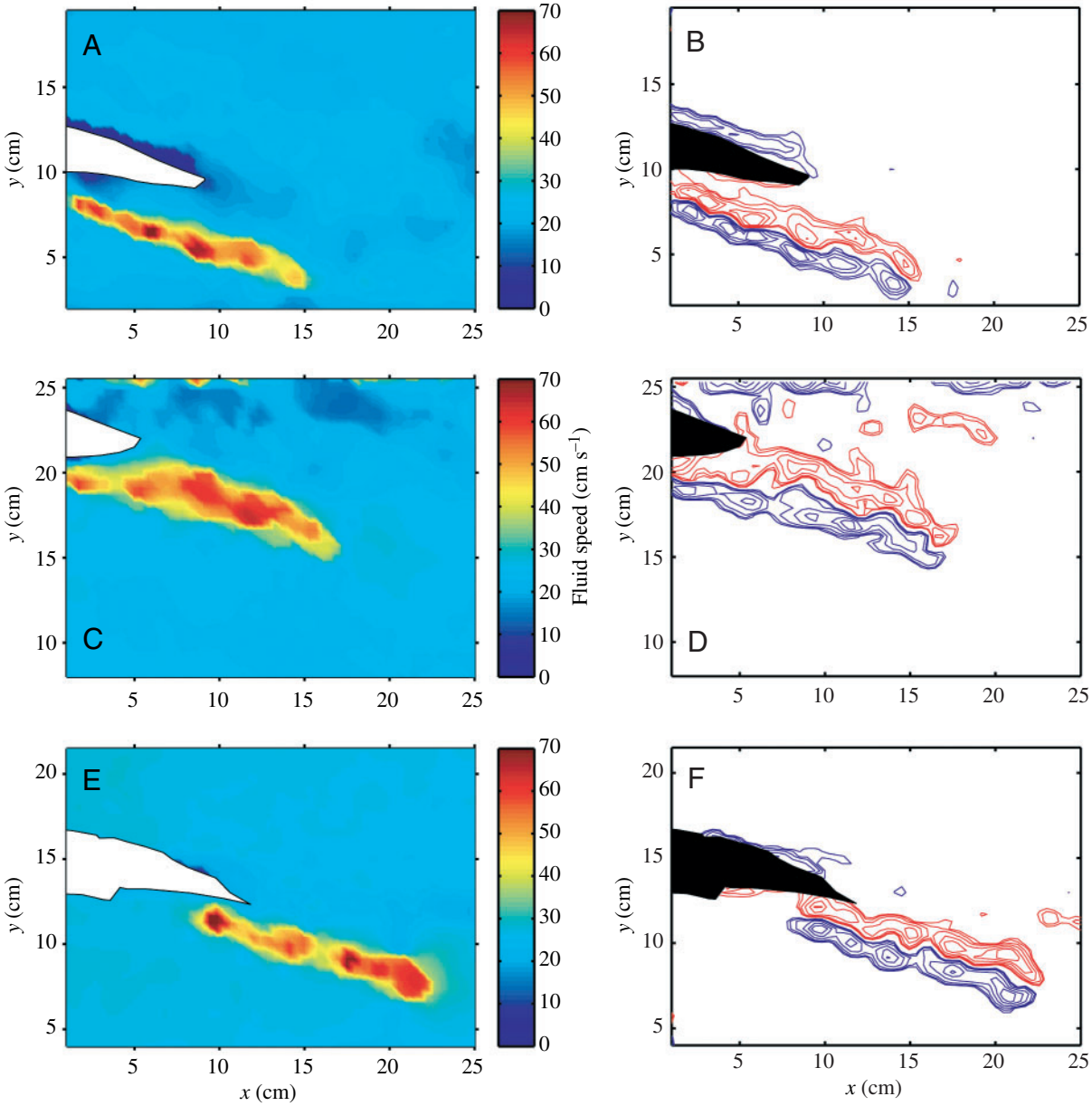

Fig. 4. Velocity magnitude (A,C,E) and vorticity contour plots (B,D,F) during three jets from three different adult *L. pealei* holding position at approximately the same swimming speed. (A,B) 25 cm s^{-1}, (C,D) 26 cm s^{-1}, (E,F) 27 cm s^{-1}. The magnitudes of vorticity contours are (B) 4, 6, 10, 15 and 20 rad s^{-1}, and (D,F) 3, 4, 6, 10, 15 and 20 rad s^{-1}. See explanation of contour identification in Fig. 2. (A,B) t=0.3 s, $t/\Delta t_j$=0.5, (C,D) t=0.3 s, $t/\Delta t_j$=0.5, and (E,F) t=0.7 s, $t/\Delta t_j$=1.2.

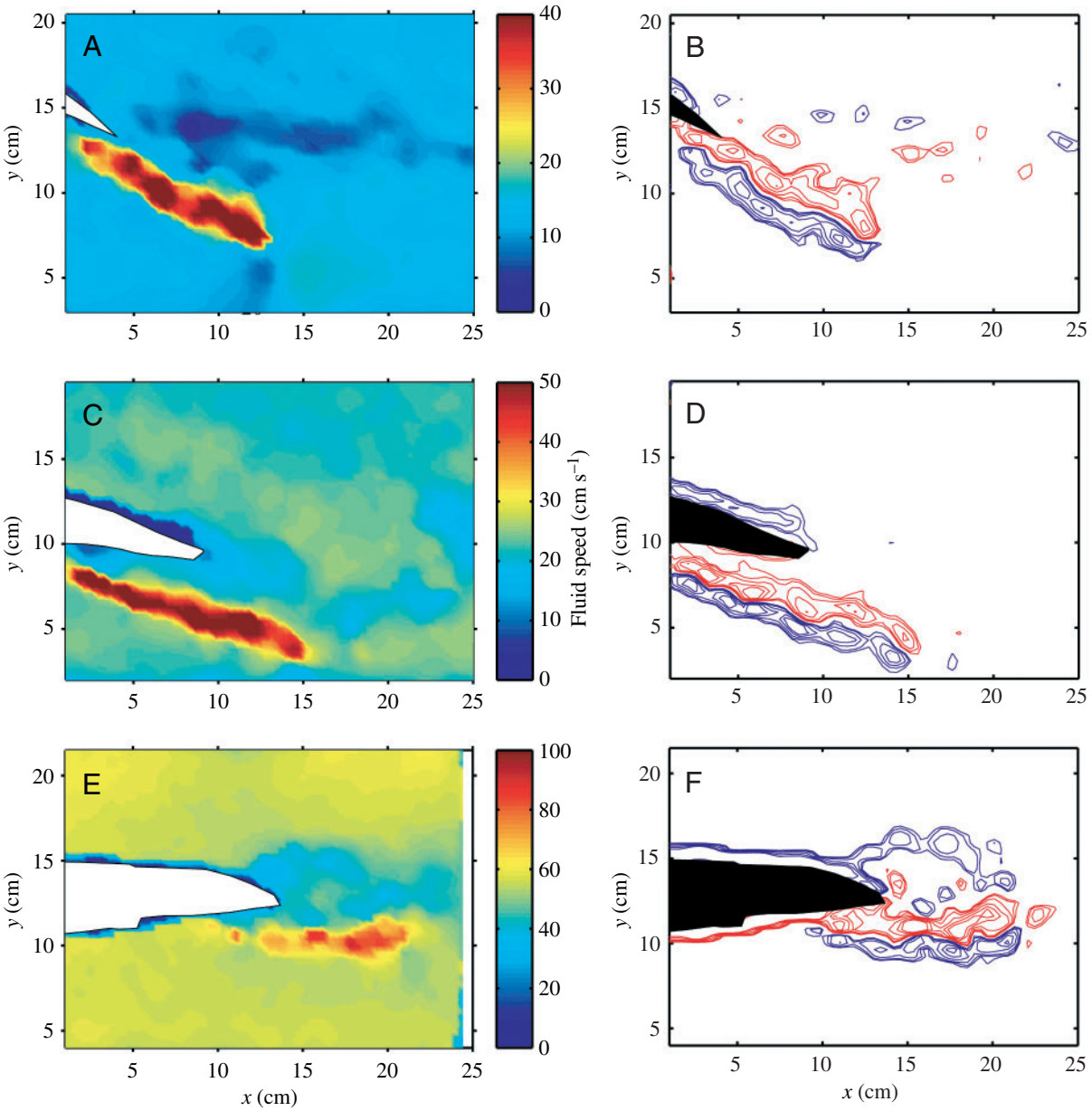

Fig. 5. Velocity magnitude (A,C,E) and vorticity contour plots (B,D,F) during three jets from three different adult *L. pealei* holding position at three different swimming speeds. (A,B) 13 cm s^{-1}, (C,D) 25 cm s^{-1}, (E,F) 56 cm s^{-1}. Note the decrease in jet angle subtended from the horizontal with increasing swimming speed. The magnitudes of vorticity contours are (B,F) 3, 4, 6, 10, 15 and 20 rad s^{-1}, and (D) 4, 6, 10, 15 and 20 rad s^{-1}. See explanation of contour identification in Fig. 2. (A,B) t=0.5 s, $t/\Delta t_j$=1.3, (C,D) t=0.3 s, $t/\Delta t_j$=0.5, and (E,F) t=0.2 s, $t/\Delta t_j$=1.0.

centers, as seen in Fig. 8A. Apparent flow reversal at the upper left-hand and lower right-hand corners are actually due to the body and wake of the squid, and the flume boundary layer, respectively. Fig. 8B,C shows the tangential and normal velocity profiles of the same jet.

L/D in squid jets

Fig. 9 shows the distribution of L_j/D for all 116 squid jets observed, where L_j is the jet structure length as observed in the field of view and D is the average jet orifice diameter during the jet period estimated to be 0.8 cm. Since L_j was greatly limited by the field of view, the values of L_j/D in just 21 of the 116 jets were considered to be good estimates (black bar areas on the histogram). These ranged from 9.0 to 29.5. L_j/D ratios for the remaining 95 jets, ranging from 4.1 to 32.0, were considered to be underestimates, even gross underestimates. In 31 of these 95, jet structure clearly extended beyond the visualized field of view. At the jet angles observed, and assuming the jet nozzle to be high up on the very upstream edge of the image, the maximum possible jet lengths that could be measured were 25.1–37.6 cm. This limits maximum measurable L_j/D ratios to 31.3–46.9. Since we attempted to capture the jet nozzle of the squid within the field of view as often as possible, measurable L_j/D ratios were further limited.

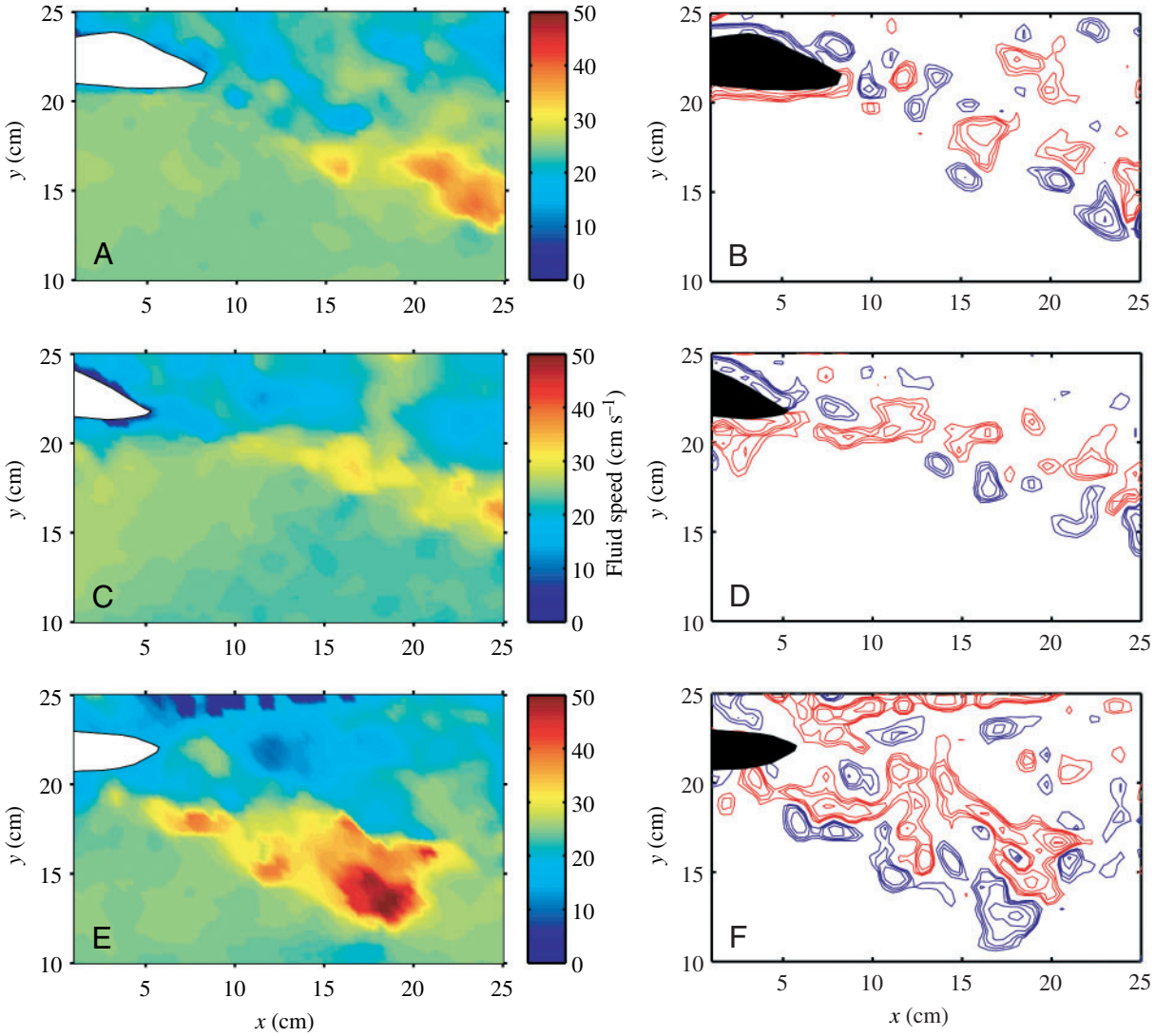

Fig. 6 .Velocity magnitude (A,C,E) and vorticity contour plots (B,D,F) showing the later development of three jets from the same adult *L. pealei* holding position at 25 cm s^{-1}. (A,B) An apparent chain of vortex-rings; (C,D) the typical jet breakdown into more or less coherent packets of vorticity; (E,F) the transition of unstable jet flow to turbulence. The magnitudes of vorticity contours are 2, 4, 6, 10, 15 and 20 rad s^{-1}. See explanation of contour identification in Fig. 2. (A,B) t=0.6 s, $t/\Delta t_j$=2.0, (C,D) t=0.53 s, $t/\Delta t_j$=1.6, and (E,F) $t/\Delta t_j$>1.0.

This is consistent with the range of L_j/D in these 31 jets (7.9 to 32.0). During 37 jets, squid exhibited yaw during jetting and therefore the jet was not aligned with the laser sheet. As mentioned in the Materials and methods, this led to a visualized jet structure that was shorter than the jet itself. L_j/D ratios in the jet visualizations affected by yaw were 5.3–27.9. In at least 24 of the 37 jets, yaw as low as 3° to 14° is sufficient to account for gross underestimates in jet length using observed jet structure diameters, D_j, of 1.0–2.5 cm. Recall that D_j is the diameter of the jet flow behind the squid, not to be confused with jet orifice diameter, D, which is taken as 0.8 cm throughout this paper. An additional 27 jets were classified as underestimates on the basis of both criteria: extension beyond the field of view and yaw. L_j/D estimates for these jets were 4.1 to 30.9. Despite these limitations, jet structure length does serve to produce an informative distribution of lower-bound jet length values for the entire data set. Most significantly, the histogram in Fig. 9 shows that the more trustworthy values (Fig. 9, black bars) characterize squid jets as elongated structures with L_j/D never less than 9.0. Jet structure lengths measured when conditions led to underestimates are grouped at the lower end of the scale. In fact, 84 of the 94 jets with L_j/D<21 in Fig. 9 qualify as underestimates, and both jets with L_j/D<5 were cases affected by both the limits of the field of view and yaw. Neither the effect of jet deceleration on jet structure length, nor stretching of the jet by the motion of the squid through the water, was examined.

Fig. 10 shows the distribution of L/D, where L is jet plug length as determined by the product of average jet velocity and jet period. This ratio is more appropriate for comparisons of our data to the data of Gharib et al. (1998). Upper- and lower-bound jet velocities, $\bar{u}_{jH}$, and $\bar{u}_{jL}$, as defined in the Materials and methods, were used to determine upper and lower bounds for plug length. L/D ratios were calculated to be 5.5–31.4 for

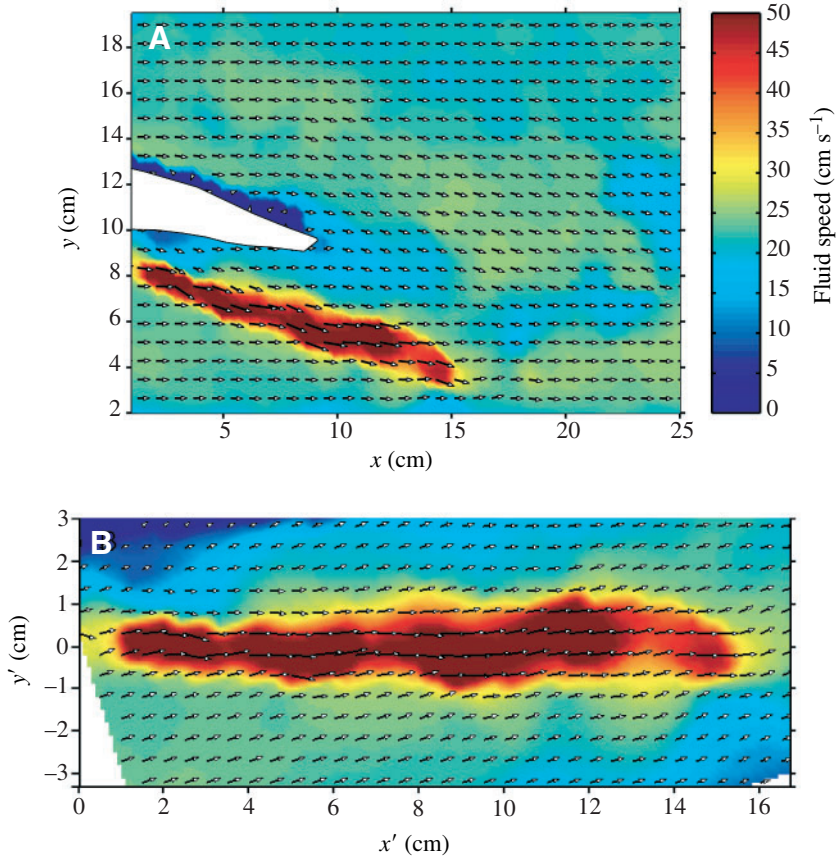

Fig. 7. (A) Representative velocity field including vectors near the aft region of a steadily swimming squid during jet emission, U=25 cm s^{-1}, t=0.3 s, $t/\Delta t_j$=0.5. In (A) the aft section of the squid is shown in white. Every other vector has been removed from the original data for clarity. (B) The sub-region of the velocity field in A surrounding the jet. The region was rotated so that the jet axis (x') is horizontal and a regular grid of vectors was interpolated at the approximate resolution of the original data. The white regions in the lower left- and right-hand corners are regions of no data.

lower-bound values (Fig. 10A), and 5.9–61.8 for upper bound (Fig. 10B). A comparison of Figs 9 and 10 shows that the distribution of the underestimates of Fig. 9 is similar to the distribution of the lower-bound values of Fig. 10, while the distribution of the 'good estimates' is more similar to the upper bound. On average, the underestimates of Fig. 9 were increased by 2.9 using the lower-bound jet plug length calculation and by 13.7 using the upper-bound calculation. For example, the lowest L_j/D value (Fig. 9), which was classified as an underestimate, jumped from 4.1 to between 26.3 and 44.9.

Jet parameters as a function of swimming speed

Fig. 11 shows the variation of several parameters of squid jet propulsion with increasing swimming speed. Trend lines and their equations are included in several of the plots, but are only meant to aid in the discussion. They should not necessarily be interpreted as equations that we consider to express the actual relationship between the variables, nor is it expected that the data should have converged strongly to a line or curve. Average jet velocity $\bar{u}_j$ (Fig. 11A; 'standard value' from the Materials and methods) increased from 19.9 cm s^{-1} to 85.8 cm s^{-1} as swimming speed U increased from 14.2 cm s^{-1} to 59.3 cm s^{-1}. Fig. 11B demonstrates that scaling jet and swimming velocities by squid mantle length do not significantly affect the trend observed in Fig. 11A. Maximum instantaneous fluid velocities observed within squid jets (not shown) ranged from 25.6 cm s^{-1} at a swimming speed of 10.1 cm s^{-1} to 136.4 cm s^{-1} at a speed of 25.8 cm s^{-1}.

Ratios of L/D calculated from average jet velocity $\bar{u}_j$, orifice diameter D, and jet period appeared to increase with increasing swimming speed, but there was considerable variability at speeds between 0.8 and 1.4 L_m s^{-1} (Fig. 11C). Fig. 11D reveals that a significant degree of that variability arises from variability in jet period. However, jet period differs from L/D in that it decreases somewhat with increasing swimming speed. This reveals that the increase in L/D with increasing swimming speed is not due to the jet orifice being open longer. Instead, it is due to increasing jet velocities, $\bar{u}_j$ (Fig. 11B). Jet frequency f (Fig. 11E) also exhibits increased variability at medium speeds, while values averaged over three or more cycles for the same squid and speeds, f_{avg}, reveal an interesting trend. Average frequency f_{avg} lies between 0.8 and 1.2 Hz and is highest at the lowest and highest swimming speeds observed. A parabolic fit to f_{avg} predicts a minimum average jet frequency at about 0.9 L_m s^{-1}.

Anderson and DeMont (2000) reported an increase in jet frequency as swimming speed increased from 1.0 to 1.7 L_m s^{-1}. Yet, their data suggested that the increase in frequency was achieved by varying primarily the refill period. Fig. 11D suggests, however, that changes in jet period are also responsible for the trend in jet frequency. In fact, we found that trends in both jet period and refill period as percentages of the total locomotive period were relatively constant near 31% and 46%, respectively, for the swimming speeds observed, with significant variability at medium speeds. The remaining 23% of the cycle represents the period during which the jet was opening and closing. Therefore, shorter locomotive periods at high and low swimming speeds were achieved by shortening both the refill and jet periods. Interestingly, for the medium speeds, at which considerable variability in jet frequency was observed, shorter locomotive periods were achieved by decreasing the percentage of the locomotive period taken up by refill while increasing the fraction taken up by opening, closing and jetting.

Jet angle β decreased with increasing swimming speed (Figs 5, 11F). This is undoubtedly related to the maintenance of a relatively constant upward component of jet thrust to counter the squid's constant negative buoyancy. The higher jet

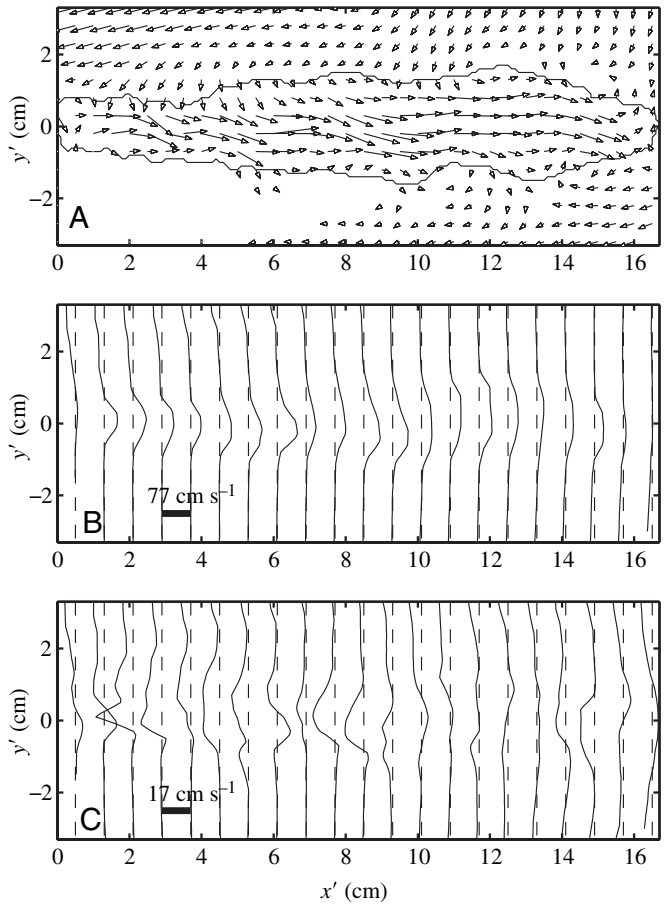

Fig. 8. (A) Velocity field, (B) tangential profile and (C) normal profile of the jet from Fig. 7 with freestream flow velocity subtracted. The velocity magnitude contour in A reveals the jet structure as defined in this work as the locus of points for which velocity drops to within 5% of the freestream flow. Blank grid points represent locations of zero relative velocity. Broken lines in profile plots (B,C) are profile axes. Profiles are solid curves. Profile values to the right of axis of a given profile in B and C represent flow in the positive x'- and y'-directions, respectively, in the rotated reference frame.

velocities $\bar{u}_j$ at higher swimming speeds produce a greater thrust along the axis of the jet. If the jet angle were not decreased the squid would move up in the water column. Negative buoyancy has been measured in several squid, including *Loligo forbesi* (Denton, 1961) and *Ommastrephes sagittatus* (Zuev, 1963). At higher speeds the squid may also be capitalizing on increased lift to support its weight, further decreasing the jet angle necessary for maintaining constant vertical position. Zuev (1965) investigated the squid body as an airfoil and observed lift in experimental models. Such factors suggest that jet angle should asymptotically approach zero with increased swimming speed, and indeed, a natural logarithmic curve fit our jet angle data better than a straight line. O'Dor (1988) and Bartol et al. (2001b) have observed a decrease in angle of attack of the body with increasing swimming speed in steadily swimming squid, further suggesting the importance of lift in the balance of vertical forces.

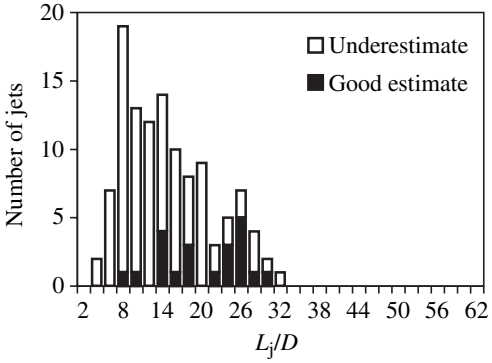

Fig. 9. Histogram of the ratio of jet structure length to jet diameter, L_j/D, based on the maximum length of each jet in the field of view visualized for all squid jets in which the squid was holding position (116 jets). The black section of each bar represents measurements that appeared to be good estimates of the total length of the jet structure. The white section of each bar represents measurements considered to be underestimates because the jet structure extended out of the field of view or the squid swam at a slight angle to the laser plane. Bin centers start at 2 and bin width is 2.

Propulsive efficiency

Fig. 12A shows slip as a function of swimming speed based on the average jet velocity $\bar{u}_j$, and the component of the flume flow in the direction of the jet, $U\cos\beta$. A broken line shows the trend if jet angle β is ignored. The trend-lines for slip calculated with and without considering jet angle vary less as speed increases (Fig. 12A), since jet angle decreases with increased swimming speed (Fig. 11F). The average difference between the two calculations of slip for our data was 10%. Either way, the data suggest a decrease in slip with increasing swimming speed, asymptotically approaching 0, which is a trend common to plots of slip in vehicles driven by jets and propellers. It reveals a relative decrease in the excess kinetic energy left in the wake with increased swimming speed, and therefore a higher propulsive efficiency. Propulsive efficiency during jetting η_j from Eq. 3 (Fig. 12B) reaches relatively high values, even at medium speeds, and then levels off. The average efficiency is 86% for speeds above 0.65 L_m s^{-1} and 93% for speeds above 1.6 L_m s^{-1}, with efficiencies for a handful of jet events reaching 95–97% at speeds above 0.9 L_m s^{-1}. These values may be slightly high since the standard jet velocity used in the calculation of efficiency may underestimate true jet velocity. Fig. 12C confirms that propulsive efficiency calculated from Eq. 3 (broken curve) matches very nicely with that calculated from estimates of total and excess kinetic energy of the jet.

Whole-cycle hydrodynamic efficiencies η_{wc} (not shown), calculated using Eq. 4, were much lower than jet propulsive efficiency, as expected, due to the high cost of refill. Average values ranged from 42 to 49%. Anderson and DeMont (2000) report a range of 34–48%. However, taking their observed swimming speeds, jet velocities, jet angles and applying the same estimations concerning refill area and period that we used (see Materials and methods), one obtains a range of 38–44%.

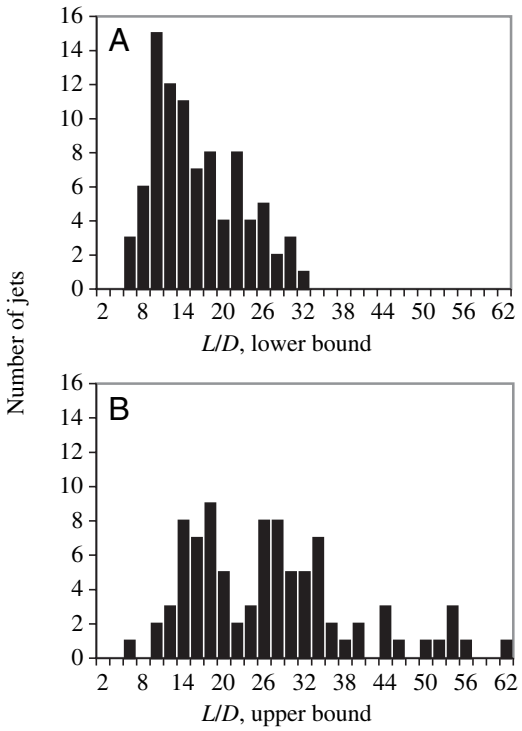

Fig. 10. Histograms of estimated upper (A) and lower-bound (B) distributions of the ratio of jet plug length to jet diameter, *L*/*D*, based on jet velocity and jet period for squid jets in which the squid was holding position and the jet nozzle was visible (89 out of 116 jets). Bin centers start at 2 and bin width is 2.

Their lower-bound value of 34% was obtained because they purposely set the upper-bound refill velocity equal to average jet velocity. This is certainly too high, but served to predict a trustworthy lower bound for whole cycle hydrodynamic efficiency. Our observations during the refill period, however, suggest an upper-bound refill velocity closer to 0.5 times average jet velocity (see Materials and methods).

Jet thrust

Fig. 12D shows average jet thrust in squid as a function of swimming speed calculated by two methods: (1) from a three-dimensional approximation of the change in momentum per time between successive visualizations of jets, and (2) using the upper-bound jet velocity in the simplified steady equation for jet thrust along the jet axis (i.e. $\rho A u_j^2$, where ρ is the density of seawater, A is the cross-sectional area of the jet, u_j is the magnitude of the jet velocity). Both methods can only be considered approximations in comparison to jet thrust determined from the actual jet velocity at the jet orifice and the orifice area as functions of time, as in Anderson and DeMont (2000). Nevertheless, their average jet thrust of 0.030 N determined in a squid swimming 1.0 L_m s^{-1}, including unsteady effects, falls within the range of our estimates from velocity and momentum of 0.017 to 0.042 N. This agrees well with the necessary average jet thrust of approximately 0.030 N determined by Anderson et al. (2001c) from the acceleration of and drag on similarly sized squid during jetting at the same swimming speed (see their Fig. 10). We used our upper-bound jet velocity in Fig. 12D because it was closer to the more reliable measurements of Anderson et al. (2001c).

Jets from pipes with background flow

So far, we have focused on jets of squid without much mention of the impact of background flow. Flow visualization of jets emitted from pipes revealed the important role of background flow in the development of the fluid structure of squid jets. As described earlier, our pipe jet results for jets emitted into still water (U=0) matched the findings of Gharib et al. (1998) (Fig. 2). Fig. 2A shows the predicted formation of a single vortex ring when *L*/*D*=4.3. By contrast, Fig. 2B shows that a trail of vorticity follows the leading vortex ring when *L*/*D*=16. In both cases, piston velocity u_p was 5 cm s^{-1}, but since, U=0, the ratio of background flow velocity to piston velocity, U/u_p, was zero. Fig. 13 illustrates the impact of increasing levels of background flow on jet structure. The ratios of background flow to piston velocity shown are 0.5, 1.0 and 2.0, respectively. Even at the lowest level of non-zero background flow (U/u_p=0.5), jet structure (Fig. 13A,B) was different from the still-water case (Fig. 2A,B). When *L*/*D*=4.3 (Fig. 13A) there was no longer a single, well-defined vortex ring as in still water (Fig. 2A). Instead, jet vorticity was spread over a distance of about 10 cm and suggested a deformed leading vortex ring with some trailing vorticity. At *L*/*D*=16 (Fig. 13B), the leading vortical structure was also deformed and slightly less prominent than observed in still water (Fig. 2B). Only slight remnants of vorticity originating from the outer boundary layer and of magnitude comparable to jet vorticity were present around the jet flow (Fig. 13A,B). At the next level, in which background flow velocity was equal to piston velocity, U/u_p=1.0 (Fig. 13C,D), the effects observed in Fig. 13A,B were much more obvious. For the case of *L*/*D*=4.3 (Fig. 13C), all of the jet vorticity was now spread out into an elongated structure. There is little to no suggestion of a prominent leading vortex ring as in Figs 2A and 13A. When *L*/*D*=16 (Fig. 13D) the prominent leading vortex, as seen in still water (Fig. 2B), is diminished, or not observed. More significant remnants of the outer boundary layer are visible at U/u_p=1.0 than at U/u_p=0.5. Finally, when background flow velocity is twice the piston velocity, U/u_p=2.0 (Fig. 13E,F), the outer boundary layer vorticity dominates and there is essentially no comparable jet vorticity present. Although this level of background flow is not assumed to be generally applicable to squid, it helps to illustrate a continuum in the relative levels of dominance of the inner and outer boundary layer vorticities as the level of background flow, U/u_p, is increased.

The structure of squid jets resembled that of the pipe jets with background flow levels of U/u_p=0.5–1.0 with large *L*/*D* ratios (Fig. 13B,D). The level of background flow expressed as the ratio of component of the swimming speed in the direction of the jet to the average jet velocity over the entire jet structure, $U\cos\beta/\bar{u}_{jL}$, is 0.5 to 0.9 in all but 6 of the 116 squid jets

analyzed. The 6 exceptions were all jets at the lowest swimming speed, with ratios of 0.4. The average for all jets observed is 0.71. If the standard value for average jet velocity, $\bar{u}_j$, is used, 95 of 116 jets exhibit ratios of background flow to jet velocity, $U\cos\beta/\bar{u}_j$, of 0.5 to 0.85, with an average of 0.58 for all 116 jets. This can be seen in the plot of slip $u_j/U-1$ (Fig. 12A), which shows that only 21 jets have a slip of greater that 1 (i.e. $U/u_j<0.5$). Recall that slip was calculated using $\bar{u}_j$ ('standard' value) for u_j and $U\cos\beta$ for U. In general, the jets of Figs 13B and 13D look slightly more stable than squid jets, but this most likely reflects the fact that (1) Reynolds number was roughly 1/4 times the value of that in squid, (2) the experimental environment was more 'quiet' and controlled, (3) cylindrical pipes are a less complicated geometry than the biological shape, and (4) jet angle was zero.

It should be mentioned here that the degree to which background flow affects jet structure is specific to the geometry of the jet-producing mechanism for a given value of U/u_p. In reality, the relative strength of the vorticity near the walls on the inside and outside of the jet nozzle is not purely a function of the level of background flow. More precisely, it is linked to boundary layer development (Prandtl, 1952; Schlichting, 1979; Fox and McDonald, 1992). The magnitude of vorticity in the boundary layer near a surface is strongly linked to the tangential velocity gradient at the surface. This explains why jet vorticity dominates in Fig. 13C,D, even though background flow velocity is equal to piston velocity. The tangential velocity gradient generally decreases near a surface as the boundary layer develops and increases in thickness over a length of that surface (Fox and McDonald, 1992). Hence, vorticity decreases. Outside of the pipe, in our experiments, the boundary layer had a relatively long distance (1–3 m) over which to develop. Inside the pipe, however, the fluid only moved along a length on the order of the piston travel (10–40 cm). Since the boundary layer has less distance over which to develop, the inner boundary layer could easily have had greater vorticity near the wall even when the piston velocity is equal to the background flow velocity. Furthermore, as the piston gets closer to the end of the pipe the vorticity of the inner boundary layer near the orifice will actually start to increase because the velocity profile near the piston is nearly uniform. That is, the boundary layer is very thin near the piston and therefore the velocity gradient near the inner wall is very high. In addition, the growth of the inner boundary layer

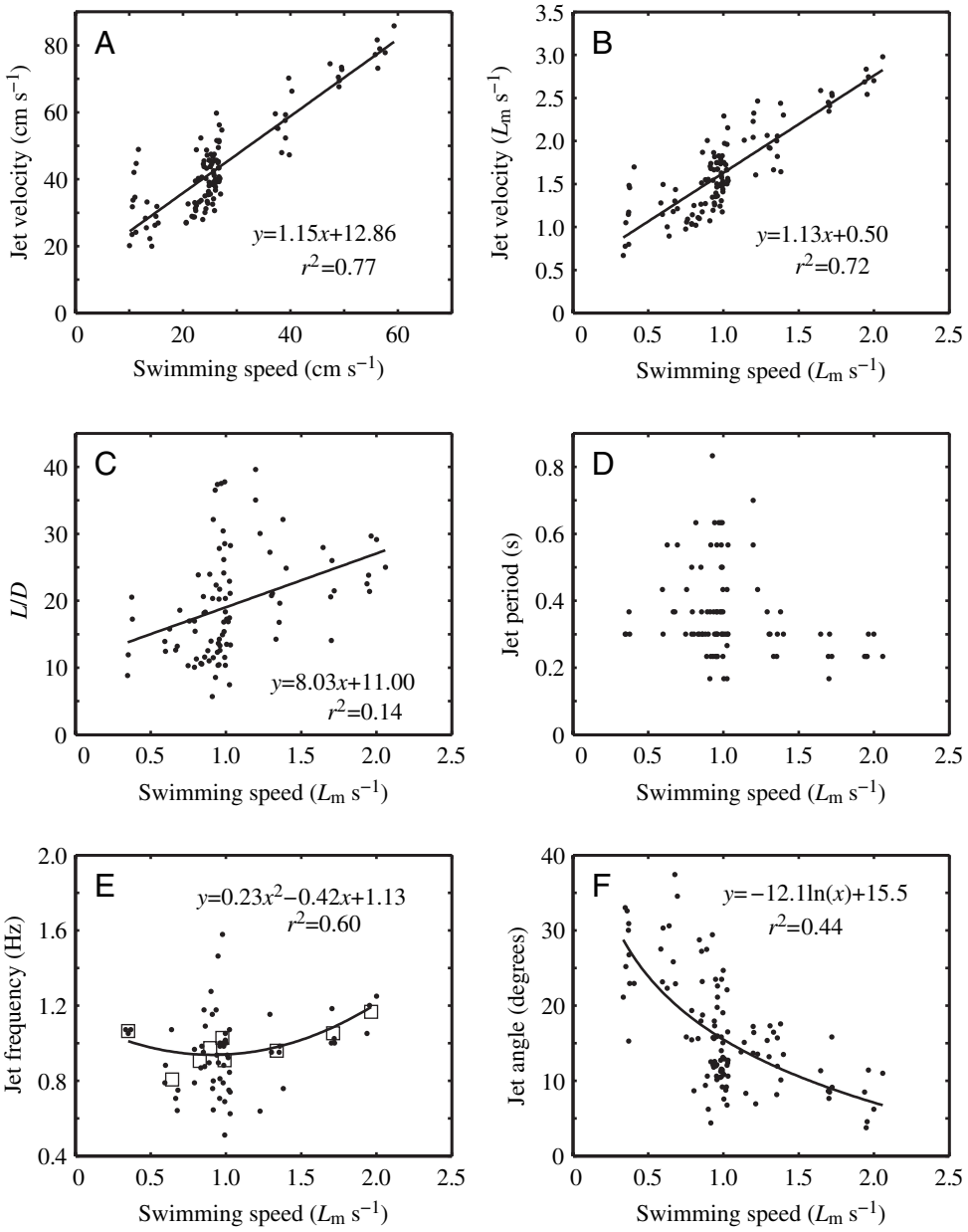

Fig. 11. (A,B) Average jet velocity $\bar{u}_j$, (C) L/D from average jet velocity, $\bar{u}_j$, jet period and jet diameter, (D) jet period, (E) jet frequency and average jet frequency, and (F) jet angle as functions of swimming speed. Swimming speed is in L_m s^{-1}, except in A. Each data point represents a jet. Jet period (D) looks discretized because of the precise timing of image exposures. In E, the open squares represent average jet frequencies, f_{avg}, for all sets of 3 or more jet events of individual squid at the same swimming speed. The curve in E is a parabolic fit to the average jet frequencies, f_{avg}. Jet angle (F) is measured in degrees subtended from the horizontal.

requires that flow toward the center of the pipe must increase above the piston velocity due to incompressibility (Prandtl and Tietjens, 1934). This can also result in steeper velocity gradients inside the pipe compared to outside the pipe. Since the geometry of the mechanism that produces squid jets is different from that of a pipe and piston, it would not be surprising if the same background flow levels did not show the same jet structure. The fact that there seems to be correspondence between background flow levels and their effect in our squid and pipe jets suggests a fortunate interplay of the geometries, mechanisms and Reynolds numbers. Nevertheless, as background flow level in jetting is increased from 0 to some value greater than 1, the transition of dominance from the vorticity shed at the inner wall to the outer wall in the downstream fluid structure is expected. Many factors, such as jet angle, jet position on the body, even angle of attack, which could also affect outer boundary layer development, may impact the degree to which background flow affects jet structure in squid.

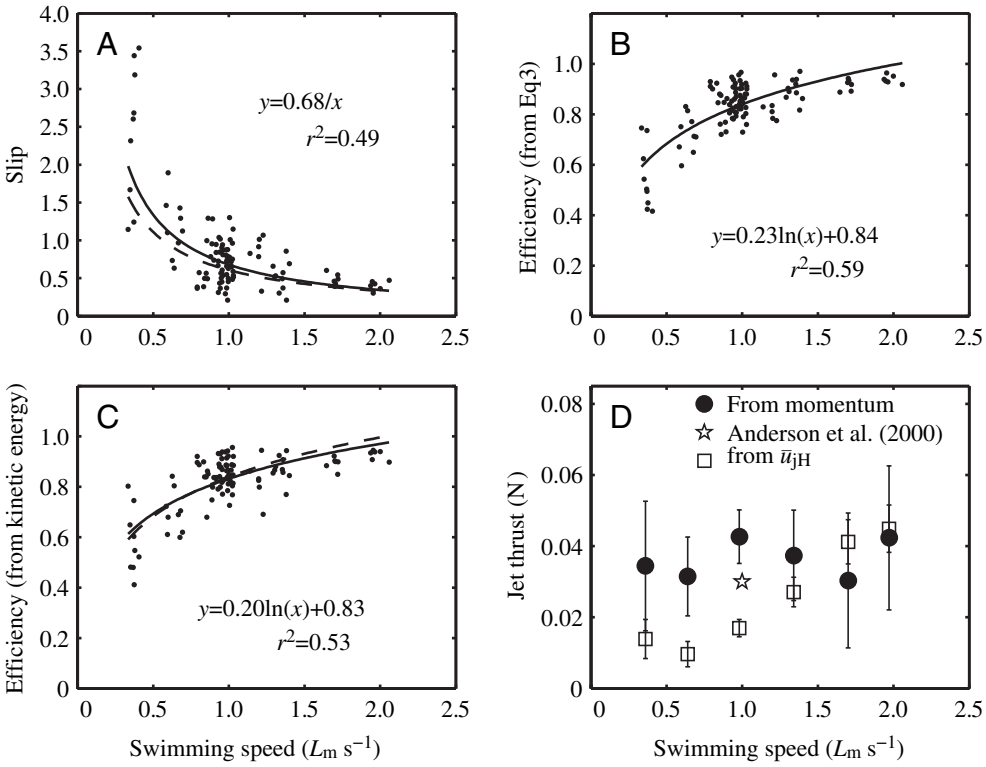

Fig. 12. (A) Slip, (B,C) propulsive efficiency and (D) jet thrust as functions of swimming speed. Equations of curve fits, when shown, are for solid curves. (A) Slip calculated as $u_j/(U\cos\beta)-1$ (data points and solid curve) and $u_j/U-1$ (broken curve). (B) Jet propulsive efficiency as calculated from Eq. 3. (C) Jet propulsive efficiency as calculated from a three-dimensional approximation of jet kinetic energy (data points and solid curve) with the fit curve from (B) for comparison (broken line). (D) A comparison of average jet thrust determined from jet velocity, the change in momentum in successive jet visualizations, and the unsteady jet analysis of Anderson and DeMont (2000). Error bars represent 95% confidence limits.

Discussion

The jets of steadily swimming, adult *L. pealei* are periodic emissions of fluid in prolonged and steady streams with plug lengths on the order of tens of orifice diameters in length. This agrees with results obtained by independent methods (Anderson and DeMont, 2000). Anderson and DeMont (2000) measured jet plug volume, $\forall$, to be 27 ml in steadily swimming adult *L. pealei* in consecutive jets at 1.0 L_m s^{-1} with an average jet nozzle diameter, D, of 0.8 cm. The rate of outflow and changes in the jet nozzle were smooth – not pulsed in anyway – during each jet event. In that case, treating plug volume as a cylinder $L=\forall/\pi(D^2/4)$, one calculates the ratio L/D to be 67.2, slightly higher than our upper-bound value of 61.8. Using our definition of jet period (i.e. the time during which the orifice was fully open), which was on average 58% of the period from jet opening to jet closing, the L/D estimate from Anderson and DeMont (2000) becomes 39.2, which is well within the range of values observed here. The fact that this value falls in our upper-bound range is not surprising since volume flow, if measured accurately, would certainly be expected to give an accurate estimate of plug flow, while our estimates based on average velocities in the jet structure are most likely underestimates.

Jet wakes and background flow

Squid and pipe jets with background flow develop differently, both spatially and temporally, compared to jets of similar plug length emitted into still water. Nevertheless, they exhibit features commonly associated with jet instability and break down. Pipe jet experiments suggest that the effects of background flow velocity are more important than the ratio L/D to predict jet structure. In a trivial sense, larger L/D ratios predict longer jet structures, but as shown in Fig. 13C,D, at sufficient levels of background flow, the general structure of the jet is basically the same regardless of L/D. Recent comprehensive studies of jets with background flow show that L/D can still be used, but only if it is made a function of background flow level (Jiang and Grosenbaugh, 2002; Krueger et al., 2002, 2003). For instance, in Fig. 13A (L/D=4.3, U/u_p=0.5), the piston stroke L could have been decreased so that the vorticity trailing the leading vortex ring would not be

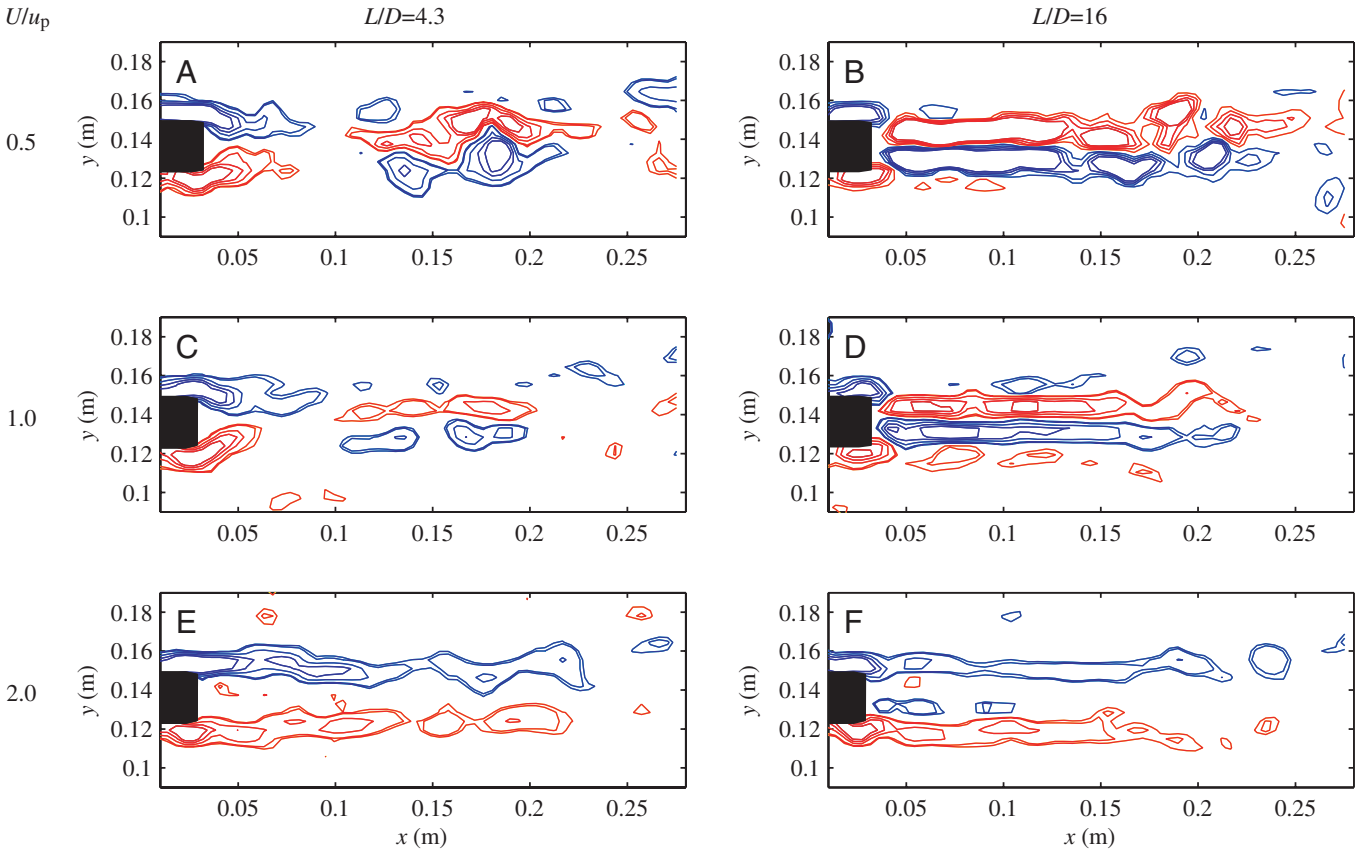

Fig. 13. Vorticity contour plots of pipe jet events with increasing levels of background flow (U/u_p) for the cases of L/D=4.3 (A,C,E) and L/D=16 (B,D,F). (A,B) Background flow velocity less than piston velocity, U/u_p=0.5 (U=5 cm s^{-1}; u_p=10 cm s^{-1}; D=2.39 cm). (C,D) Background flow velocity equal to piston velocity, U/u_p=1.0 (U=5 cm s^{-1}; u_p=5 cm s^{-1}; D=2.39 cm). (E,F) Background flow velocity greater than piston velocity, U/u_p=2.0 (U=5 cm s^{-1}; u_p=2.5 cm s^{-1}; D=2.39 cm). The magnitudes of vorticity contours are 0.4, 0.5, 1.0, 1.5 and 2.0 rad s^{-1}. See explanation of contour identification in Fig. 2. (A) t=3 s, $t/\Delta t_j$=3, (B) t=3 s, $t/\Delta t_j$=0.8, (C) t=4 s, $t/\Delta t_j$=2, (D) t=4.7 s, $t/\Delta t_j$=0.6, (E) t=8 s, $t/\Delta t_j$=2, and (F) t=6 s, $t/\Delta t_j$=0.4.

present. Hence, the ratio L/D at which only a vortex ring is formed is lower when background flow is present than in still water. Of course, the jet thrust and total circulation associated with such a vortex are less than those of a vortex produced in still water with L/D=4, assuming jet velocity to be the same. Therefore, in order for an organism to maintain periodic vortex ring propulsion, it must make adjustments to its locomotive behavior as swimming speed, i.e. background flow, increases. In particular, the organism must reduce jet plug length and/or increase jet velocity. A reduction in jet plug length alone would decrease the momentum output per jet, and the frequency of jetting and/or jet orifice area would need to be increased to maintain the same average thrust. These strategies would be necessary as the organism approached its maximum sustainable (i.e. aerobic) jet velocity. Below maximum jet velocity, an organism could increase jet velocity in an attempt to decrease the effects of background flow in vortex ring formation, or use a combination of increased jet velocity, frequency and orifice area. However, these adjustments have potential drawbacks. Increased jet velocity in comparison to background flow usually results in more wasted kinetic energy in the wake, thus decreasing efficiency. Furthermore, maximum swimming speed could be unduly limited by the need to keep swimming speed low compared to jet velocity. Our pipe jet experiments suggest that jet velocities greater than 2 times swimming speed would be necessary to maintain individual vortex ring production at L/D=4, whereas adult squid were observed to swim at fast speeds (2.0 L_m s^{-1}) with jet velocities just 1.4 times swimming speed (slip=0.4, Fig. 12A). Increased jet frequency can result in greater energy costs as well, due to unsteady fluid forces associated with more frequent accelerations of both the surrounding fluid and working fluid. The net contribution of unsteady forces to overall thrust appears to be small in steady swimming squid (Anderson and DeMont, 2000), but the increased effort and energy needed to power them is unavoidable. That is not to say that propulsive systems that can make such adjustments do not exist, but it seems an unlikely mode of locomotion for fast, steadily swimming jet-propelled organisms. Adult *L. pealei* certainly do not exhibit such behavior in steady swimming. Hence, the periodic vortex propulsion models such as those of Siekmann (1963) and Weihs (1977) should be used cautiously when analyzing jet-propelled organisms where the potential for significant background flow is present.

In light of the preceding discussion, it is not surprising that slower, smaller organisms (Bartol et al., 2001b), hovering organisms (Rayner, 1979), and swimmers that decelerate significantly before jetting, such as medusae (Prandtl, 1952; Colin and Costello, 2002) have been reported to use vortex ring propulsion. Periodic vortex ring models (Siekmann, 1963; Weihs, 1977; Ellington, 1984) may apply in many such cases. Nevertheless, there are some very interesting fast-moving exceptions, namely, animals that propel themselves by flapping fins and wings. The presence of vortex rings and vortex ring-like structures in the wakes of such animals is well documented (Lighthill, 1969; Spedding et al., 1984; Blickhan et al., 1992; Drucker and Lauder, 2000). Interestingly, flapping propulsion is characterized by an assortment of the very behaviors posed above for maintaining vortex ring production in the presence of significant background flow: high jet frequency, high jet velocity and/or large jet cross-sections. At the same time, there is interesting evidence that speed, and therefore possibly background flow, impacts jet fluid structure, even in these organisms. In birds and bats, a clear transition in the wake structure from a vortex ring gait to a continuous vortex gait with increasing flight speed has been described by Rayner (1988, 1995). Although the fluid dynamics are quite different from those of squid propulsion, the pattern of (1) vortex ring propulsion at lower speeds and (2) a more elongated structure at higher speeds, suggests that increased background flow may limit the practicality of propulsion by individual vortex rings. The same conclusion might be drawn from a consideration of the wake of individual vortex rings shed from pectoral fins in labriform locomotion (Drucker and Lauder, 2000) and the chain-like vortex wake shed from the caudal fin of a tuniform swimmer (Nauen and Lauder, 2002). In fact, in high-speed labriform swimming, the wake shed from pectoral fins transitions from individual vortex rings, to pairs of linked vortex rings (Drucker and Lauder, 2000).

Our work, viewed together with the work of Bartol et al. (2001b), lends strong support to a similar transition from vortex ring wakes to elongated jet wakes in squid as they move from juvenile to adult stages of development. Our results suggest that longer jet plug lengths occur at higher swimming speeds in adult squid. If small squid are, instead, tuning jet plug length for pulsed vortex ring production, when in the lifetime of the squid does the transition take place? Is it characterized by a gradual change in jet structure or an abrupt change at some stage of development? Is there a clear transition in the body kinematics in steady swimming? What are the fluid dynamic parameters associated with the transition, such as Reynolds number and slip? Does transition depend on a parameter related to background flow and jet speed, or is it determined by physiological constraints such as mantle cavity volume and muscle power?

Squid jet structure and efficiency

One obvious question about the fluid structure of jets in squid is whether propulsive efficiency plays a role in the determination of an elongated jet *vs* periodic vortex ring propulsion. Recall that Linden and Turner (2001) predict that vortex rings produced at an *L*/*D* ratio of about 4 are characterized by the highest ratio of thrust to jet plug kinetic energy, and that Krueger and Gharib (2003) reported that thrust produced by a jet is augmented when a vortex ring is produced. Since useful work in Eq. 1 is defined as thrust times forward velocity, *TU*, when used to determination propulsive efficiency, these findings regarding optimized thrust strongly suggest vortex ring propulsion as more efficient that an elongated jet. Krueger and Gharib (2003) do report, however, that a significant volume of fluid in excess of the jetted fluid is set into motion during vortex ring formation and one might ask what contribution this makes to 'wasted kinetic energy' in the wake, which by Eq. 1, decreases efficiency. Nevertheless, it is difficult to imagine that additional fluid set into motion by the phenomenon of over-pressure, which they describe, would increase wasted kinetic energy to the degree that it would outweigh the contribution of augmented thrust to propulsive efficiency. However, our data show that slip in squid decreases significantly with increasing swimming speed (Fig. 12A). Therefore, as *TU* increases in elongated jet locomotion by squid, wasted kinetic energy decreases proportionately. Recall that we calculated average propulsive efficiency during the jet period to be 86% for speeds above 0.65 L_m s^{-1} and 93% for speeds above 1.6 L_m s^{-1} (Fig. 12B,C). It is possible that at some speed, the efficiency gains due to an elongated jet with low slip outweigh those of propulsion at the same swimming speed by a vortex ring or series of rings emitted from the same jet orifice cross-section. Extrapolating the trend in slip suggests that the elongated jet of squid approaches a state in which jet velocity is equal to background flow, that is, approaches zero wasted kinetic energy from the jet in the wake and 100% propulsive efficiency. Hypothetically, with help from the fins, or an extremely low drag coefficient, the squid could come very close to this state. However, the inner and outer boundary layers of the jet nozzle make some degree of slip, and therefore wasted kinetic energy, inevitable. Interestingly, numerical simulations by Jiang and Grosenbaugh (2002) predict that hydrodynamic efficiency increases with increasing *L*/*D* in the presence of background flow, and as mentioned earlier, *L*/*D* in adult squid increases with increased swimming speed (Fig. 11C). Therefore, squid may be gaining an added benefit at higher speeds due to the mechanism they propose. By contrast, in vortex ring propulsion where *L*/*D* is near 4, high jet velocities required due to background flow and circuitous streamlines make it impossible to reach even a theoretical state of 0 wasted kinetic energy. Certainly, more data is needed to determine absolute propulsive efficiencies of the two jet types in the presence of background flow, but it is not clear that vortex ring propulsive efficiency is dramatically greater, or even always greater, than elongated jet propulsive efficiency with increasing background flow. Regardless of any possible role played by differences in propulsive efficiency between the two modes, we suggest that the use of elongated jets may be understood in the context of the following factors: (1) the physiological, fluid dynamic and energetic limitations that

discourage high frequency jetting, (2) the effects of background flow, (3) the increased power per jet event offered by a high volume jet output, and (4) the complementary relationship between the squid's jet, as a high-power propeller, and the squid's fins, as high-efficiency propellers.

Squid have often been assigned low propulsive efficiency on theoretical grounds – that accelerating a small mass of fluid as a high-speed jet is less efficient than accelerating a large mass of fluid as a low-speed jet (Alexander, 1968; Lighthill, 1969). However, our data suggest that squid are not in the former group. Instead, squid expel a large mass of fluid, and at relatively low speed (i.e. low slip) at swimming speeds above 0.6 L_m s^{-1}. Lighthill (1969) states that the narrowness of the jet, that is, the small orifice area, implies low efficiency. But he also assumed that jet velocity was much higher than the swimming speed, or background flow. Certainly, a larger jet orifice would theoretically allow for equivalent average thrust at lower slip, but this would require higher mass flow rates and overall mass emitted. In fact, regardless of a change in orifice area, lower slip requires greater volume output, period. In simple terms, by conservation of momentum, a squid receives momentum equal and opposite to the momentum of the jet fluid ejected. Since drag continuously saps that momentum from the squid, the squid must output a certain amount of momentum per locomotive period to maintain a constant average swimming speed. To maintain a particular swimming speed and decrease jet velocity (i.e. decreasing slip), regardless of orifice area, the squid must output more mass per locomotive cycle to emit the needed momentum. This could be accomplished by increasing the jet period rather than the jet orifice area, resulting in a lower volume flow rate. But this assumes that the locomotive cycle has time to spare and requires an increase in refill volume flow rate, since the refill period would have to be shortened. To prevent refill losses from outweighing the gains of lower slip, the refill orifice would have to increase in size. It is tempting to suggest, however, that the squid is already operating near the optimum balance at which the gains of slip are maximized and the losses of refill are minimized, and that there is no significant amount of time to spare in the locomotive cycle. The equations of efficiency derived for squid by Anderson and DeMont (2000) and expanded here to include jet angle (Eqs. 3,4) predict that whole-cycle hydrodynamic efficiency in squid has a theoretical maximum of 58%, which occurs when refill velocity and jet angle are small, and jet velocity is 1.7 times the swimming speed, i.e. slip=0.7. We observed that average slip (taking jet angle into account) at swimming speeds above 0.6 L_m s^{-1} was 0.67 (Fig. 12A), remarkably close to 0.7, suggesting that squid are indeed jetting such that they perform near their theoretical propulsive limit at medium to high swimming speeds. This was also suggested by Anderson and DeMont (2000).

Therefore, let us consider what is necessary to decrease slip, while maintaining momentum output per cycle but not allowing jet period to lengthen. Once again, in order to decrease slip we must decrease jet velocity, and therefore, to maintain momentum flux, mass output must increase. If this is to occur in the same, or a shorter, jet period, volume flow rate out of the mantle cavity must increase during jetting. Jet orifice area must increase and the muscles of the mantle must contract faster and possibly more forcefully due to increased unsteady forces associated with necessarily higher fluid accelerations. If jet period is not changed, refill volume flow rate must still be increased as before since total output was increased. To avoid this, jet period must be shortened. But then jet orifice area must be increased further requiring even faster muscle contractions. All this suggests that there is a limited jet orifice area at which a steadily swimming adult squid can most significantly benefit from propulsive efficiency during the jet period without suffering more significant losses due to necessary adjustments in refill rates, muscle use and unsteady fluid forces. The preceding discussion suggests that an upper limit of optimal jet orifice area is linked to an interplay of available muscle strength and contraction rate, refill orifice size, mantle cavity volume, drag, and perhaps even the relative contribution of fin propulsion available. Bartol et al. (2001b) report maximum orifice diameters between 0.4 and 0.5 cm in a squid *Lolliguncula brevis* with a mantle length of 7.3 cm swimming at a speed of about 1.2 L_m s^{-1}, while Anderson and DeMont (2000) report a maximum diameter near 0.9 cm in a specimen of *L. pealei* with a mantle length of 25 cm swimming at 1.0 L_m s^{-1}. Therefore, jet diameter in *L. pealei* is twice as large, while mantle length is 3–4 times as large. By contrast, in still smaller *L. brevis* (L_m<3.0 cm), Bartol et al. (2001b) report that jet orifice diameters are relatively larger. Consistent with the above discussion, their data show that these smaller squid with larger orifices exhibit higher mantle contraction rates. This presents another interesting topic for investigation regarding scale effects in squid and how the complex interplay of the entire locomotive cycle reflects a remarkable optimization of performance within mechanical limitations.

Ironically, our analysis of efficiency in squid suggests that the jet period in squid is relatively efficient and that an enlargement of the jet orifice area, keeping squid size constant, would likely be detrimental to efficiency, in contrast to the rule of thumb (Alexander, 1968; Lighthill, 1969). Moreover, we have found that not only does mantle refill contribute directly to low efficiency, as the whole-cycle efficiency equation of Anderson and DeMont (2000) and Eq. 4 demonstrate, but refill likely plays a role in the optimization of jet orifice area and thus indirectly affects propulsive efficiency during the jet period.

Locomotive flexibility

Four measured parameters, average jet velocity, jet period, jet frequency and average jet angle, shown in Fig. 11, demonstrated significant variability at swimming speeds between 0.6 and 1.4 L_m s^{-1}. Recall that jet frequency is the inverse of the locomotive period, which is significantly affected by refill period, and is therefore only partially dependent on jet period (see Materials and methods). The variability in these four jet parameters suggests increased locomotive flexibility on the part of the squid at medium speeds and is likely evidence that thrust and directional control

by the fins at lower speeds result in more variability in the use of the jet in the overall dynamic balance. For example, we observed that at medium speeds, squid occasionally made two fin strokes during refill, rather than the usual single stroke, which allowed the squid to decrease jet frequency. More fin thrust and longer refill periods also imply higher efficiency. Squid also demonstrated higher maneuverability at speeds slower than about 1.4 L_m s^{-1}. At higher swimming speeds, it appeared necessary for squid to settle into a steady forward stride to keep pace with the flume flow. Less flexibility in gait could explain the observed convergence of jet parameters for squid swimming steadily at higher speeds. There is some evidence of less flexibility at speeds below 0.6 L_m s^{-1}. Perhaps the combination of negative buoyancy and decreased lift at low speeds requires a more steady output on the part of both the fins and the jet. It is interesting that the minimum in the trend of average jet frequency (Fig. 11E) occurs at 0.9 L_m s^{-1} where the variation in jet parameters is greatest. This is a speed at which we have observed adult *L. pealei* to swim steadily for long periods of time, even several hours, without tiring. At much lower speeds, squid hold position less readily, and at speeds greater than 1.4 L_m s^{-1}, adult *L. pealei* tire quickly. 0.9 L_m s^{-1} is also the swimming speed at which jet propulsive efficiencies begin leveling off near theoretical maximum values (Fig. 12B). These observations suggest that the preferred swimming speed of adult *L. pealei* coincides with the speed at which both propulsive efficiency and locomotive flexibility are high, and the average number of contractions of the mantle over a given period of time is lowest. It would be interesting to investigate work output as a function of contraction rate to determine if this apparent minimum in average jet frequency represents optimization of muscle use. Bartol et al. (2001a) report U-shaped O_2 consumption curves in several *Lolliguncula brevis* with a minimum value occurring at a swimming speed between 0.5 and 1.5 L_m s^{-1}.

The contribution of fin propulsion certainly needs to be factored into the dynamics and efficiencies of squid locomotion. We observed periodic vortices of varying degrees of coherence being shed from the fins of *L. pealei*, especially in visualizations when the squid was shifted laterally with respect to the laser sheet. Differentiating between fin vortices and jet structure was not difficult since the jet nozzle was visible in the majority of the jets observed. Jet structure was so consistent and so different from the structure of the vorticity shed from the fins that there was essentially no ambiguity even when the jet nozzle was not visible. No obvious interaction between the two flow structures was observed, but this does not rule out the interesting possibility of such interaction. Anderson and DeMont (2005) reported that fin gaits in adult *L. pealei* were clearly tuned to jet gait and that the two are modulated at different speeds. Anderson (1998) and Anderson and DeMont (2005) echoed the claims of Packard (1969) and O'Dor (1988) that the fin gait in steady swimming appeared to reduce deceleration during the refill period thereby reducing fluctuations in swimming speed during the locomotive cycle. In fish, potentially favorable interactions between vorticity shed from upstream structures and the main propulsor, the caudal fin, have been observed (Drucker and Lauder, 2001).

The effect of jet angle on the structure of the jet flow was not investigated here, but it could be significant on some level. For example, if a squid were to jet straight down while moving relatively fast through the water, the jet fluid would spread out over the distance that the squid moved during the jet period (i.e. undergo stretching). Since the initial momentum of each parcel of fluid ejected would be directed downward (and somewhat forward due to its original momentum from being carried with the squid itself), it is hard to imagine that all of the fluid of such a jet could possibly roll up into a single vortex ring unless it was a very short jet. We observed jet angles between 4° and 37° (Fig. 11F) and slight curving of the jet structure due to such stretching was observed in some cases. It is possible that this sort of deformation played a partial role in producing the jet structure observed in squid, especially at the larger jet angles. There was also occasional evidence of curvature in the jet opposite to what would be expected by stretching, which suggests that squid were sometimes changing the jet angle during jetting. The effect of the opening and closing phases of the jet orifice on jet structure may also have a significant impact on jet structure and calls for further investigation.

Determining jet thrust in swimming squid

The observed elongated fluid structure of the jets of adult *L. pealei* suggests that a basic application of the 'momentum equation' (Fox and McDonald, 1992), using the inside surface of the squid mantle and funnel to the face of the jet orifice as the control volume (Anderson and DeMont, 2000), is sufficiently accurate to determine jet thrust in large, steadily swimming squid. Nevertheless, there are two difficult variables in the equation: (1) an unsteady term representing the contribution of temporal accelerations and decelerations of fluid in the mantle and funnel, and (2) the velocity profile of the jet at the jet orifice. Anderson and DeMont (2000) used highly accurate volume flow data from high speed video records of steadily swimming adult *L. pealei* to calculate the contribution of the unsteady term. They found that instantaneous body acceleration more closely matched jet thrust when the unsteady term was included in the momentum equation (see Anderson and DeMont, 2000, fig. 8). However, their plot of thrust indicates that the contribution of the unsteady term to average thrust over the jet period is small in a squid swimming at 1.0 L_m s^{-1}. This is because the effects of acceleration and deceleration of fluid in the mantle cavity at the beginning and ending of the jet period, respectively, are nearly equal. Using their data, we determined the contribution of the unsteady term to average jet thrust to be less than 1%. The contribution could increase if greater quantities of the mantle fluid were expelled. For example, if all of the fluid were expelled without ever decreasing jet velocity during the jet period, no negative contribution from deceleration of fluid in the mantle would occur. A comparison of average thrusts from jet onset until peak thrust using the data found in Anderson and DeMont (2000) suggests a contribution by the unsteady term

in such an example on the order of 24%. Furthermore, they report that a squid swimming 1.7 L_m s^{-1} expelled 64–94% of its mantle cavity fluid in jet periods from a sequence of three locomotive periods. Nevertheless, at 'preferred' swimming speeds, near 1.0 L_m s^{-1}, squid expel a smaller percentage of their mantle cavity volume and the unsteady term appears to play a negligible role in average jet thrust.

The second difficult variable in the momentum equation, the velocity profile at the jet orifice, has yet to be measured. The shape of this profile ultimately determines the rate at which momentum is expelled from the jet orifice, i.e. the control volume. The instantaneous rate of momentum transfer across the surface of the control volume is equivalent to the instantaneous 'steady' contribution to jet thrust. A constant jet profile at the orifice results in a steady contribution to thrust, T_s, equal to $\rho A u_j^2 \cos\beta$. If, however, the profile is parabolic, as might be expected of a fully developed laminar jet (Fox and McDonald, 1992) steady thrust, T_s, differs by a constant factor – 1.33 for a circular orifice and 0.6 for a slit-like orifice. Fig. 1 shows that a squid orifice varies between slit-like and circular during jetting. In the case of turbulent flow, a 'flatter' profile would lead to thrusts closer to that of a constant profile compared to laminar flow. But in both cases, laminar and turbulent, the development of these profiles requires the development of inner wall boundary layers over significant lengths, and the squid funnel is quite short and, moreover, is largely a contraction. Boundary layers tend to thin in a contraction. Therefore, one might assume that the squid jet profile at the jet orifice is relatively undeveloped, or nearly constant. In that case, the simple equation, $T_s=\rho A u_j^2 \cos\beta$, using average jet velocity at the jet orifice, is probably a good estimate for the contribution of the steady term of the momentum equation to jet thrust. Fig. 12D suggests that until close-up DPIV of the jet orifice and/or accurate 3D DPIV measurements of the entire jet structure, the methods of Anderson and DeMont (2000) and Anderson et al. (2001c) yield the most reliable estimates of jet thrust.

Coincidently, most previous hydrodynamic analyses of squid locomotion used the momentum equation, and as explained above, ignored the unsteady term and assumed the jet profile at the orifice to be nearly constant (Trueman and Packard, 1968; Johnson et al., 1972; O'Dor, 1988; Bartol et al., 2001b). Our findings regarding the elongated shape of squid jet structure, together with the unsteady analysis of Anderson (1998) and Anderson and DeMont (2000), suggest that such analyses produce good estimates of average jet thrust as long as jet velocity and jet orifice area are accurately measured. This study suggests that more complicated treatments of squid locomotion, which assume periodic vortex ring propulsion, are not necessary in, or even applicable to, the analysis of large, steadily swimming squid.

List of symbols

A	jet orifice cross-sectional area
D	diameter of jet orifice, pipe inside diameter
D_j	diameter of the jet fluid structure assuming roughly circular cross-sections
f	jet frequency
f_{avg}	average jet frequency
KE_e	excess kinetic energy of jet
KE_T	total kinetic energy of jet
L	length of the plug of fluid emitted by a jet, length of piston stroke
L_j	length of jet fluid structure in the camera field of view
L_m	squid mantle length
L_s	total body length of squid
Q	rate of volume flow out of the jet orifice
T	thrust
t	time from jet onset
T_s	steady component of jet thrust
U	swimming speed or flume speed
$\bar{u}_j$	average jet core velocity or 'standard jet velocity'
u_j	instantaneous jet velocity
u_{jc}	jet core velocity
$\bar{u}_{jH}$	upper-bound average jet velocity
$\bar{u}_{jL}$	lower-bound average jet velocity
u_p	piston velocity
u_R	squid mantle refill velocity
Ψ	total volume emitted during a squid jet
x	horizontal axis of the camera frame of reference
x'	horizontal axis of the rotated camera frame of reference
y	vertical axis of the camera frame of reference
y'	vertical axis of the rotated camera frame of reference
Δt	time between image exposures
Δt_j	jet period
Δt_R	refill period
β	jet angle subtended from the horizontal
η	propulsive efficiency
η_j	jet propulsive efficiency
η_r	rocket motor propulsive efficiency
η_{wc}	whole-cycle hydrodynamic efficiency of squid
ρ	fluid density

The authors thank M. Rapo (MIT/WHOI) and K. McKenney (MIT) for many hours spent processing data, and H. Jiang (WHOI) for valuable input regarding jet hydrodynamics. This research was supported by the Office of Naval Research Grant N00014-01-10445 and the National Science Foundation IBN-0114148. This paper represents WHOI contribution number 11084.

References

Adrian, R. J. (1991). Particle imaging techniques for experimental fluid mechanics. *Ann. Rev. Fluid Mech.* **20**, 421-485.

Alexander, R. M. (1968). *Animal Mechanics*. Seattle: University of Washington Press.

Anderson, E. J. (1998). The mechanics of squid locomotion. MSc thesis, St Francis Xavier University, Nova Scotia, Canada.

Anderson, E. J. and DeMont, M. E. (2000). The mechanics of locomotion

in the squid *Loligo pealei*: Locomotory function and unsteady hydrodynamics of the jet and intramantle pressure. *J. Exp. Biol.* **203**, 2851-2863.

Anderson, E. J. and DeMont, M. E. (2005). The locomotory function of the fins in the squid *Loligo pealei*. *Mar. Behav. Physiol.* (in press).

Anderson, E. J., Jiang, H. and Grosenbaugh, M. A. (2001a). Jet flow in swimming squid. *Am. Zool.* **41**, 1380-1381.

Anderson, E. J., McGillis, W. R. and Grosenbaugh, M. A. (2001b). The boundary layer of swimming fish. *J. Exp. Biol.* **204**, 81-102.

Anderson, E. J., Quinn, W. and DeMont, M. E. (2001c). Hydrodynamics of locomotion in the squid *Loligo pealei*. *J. Fluid. Mech.* **436**, 249-266.

Bartol, I. K., Mann, R. and Patterson, M. R. (2001a). Aerobic respiratory costs of swimming in the negatively buoyant brief squid *Lolliguncula brevis*. *J. Exp. Biol.* **204**, 3639-3653.

Bartol, I. K., Patterson, M. R. and Mann, R. (2001b). Swimming mechanics and behavior of the shallow-water brief squid *Lolliguncula brevis*. *J. Exp. Biol.* **204**, 3655-3682.

Blickhan, R., Krick, C., Zehren, D. and Nachtigall, W. (1992). Generation of a vortex chain in the wake of a subundulatory swimmer. *Naturwissenschaften* **79**, 220-221.

Colin, S. P. and Costello, J. H. (2002). Morphology, swimming performance and propulsive mode of six co-occurring hydromedusae. *J. Exp. Biol.* **205**, 427-437.

Denton, E. J. (1961). The buoyancy of fish and cephalopods. *Progr. Biophys.* **11**, 179-236.

Drazin, P. G. and Reid, W. H. (1981). *Hydrodynamic Instability.* Cambridge: Cambridge University Press.

Drucker, E. G. and Lauder, G. V (2000). A hydrodynamic analysis of fish swimming speed: wake structure and locomotor force in slow and fast labriform swimmers. *J. Exp. Biol.* **203**, 2379-2393.

Drucker, E. G. and Lauder, G. V. (2001). Locomotor function of the dorsal fin in teleost fishes: experimental analysis of wake forces in sunfish. *J. Exp. Biol.* **204**, 2943-2958.

Ellington, C. P. (1984). The aerodynamics of hovering insect flight. V. A vortex theory. *Phil. Trans. R. Soc. Lond. B* **305**, 115-144.

Fox, R. W. and McDonald, A. T. (1992). *Introduction to Fluid Mechanics*, fourth edition. New York: John Wiley and Sons.

Gharib, M., Rambod, E. and Shariff, K. (1998). A universal time scale for vortex ring formation. *J. Fluid Mech.* **360**, 121-140.

Gosline, J. M. and DeMont, M. E. (1985). Jet-propelled swimming in squid. *Sci. Am.* **252**, 96-103.

Gosline, J. M., Steeves, J. D., Harman, A. D. and DeMont, M. E. (1983). Patterns of circular and radial mantle muscle activity in respiration and jetting of the squid. *J. Exp. Biol.* **104**, 97-109.

Hoar, J. A., Sim, E., Webber, D. M. and O'Dor, R. K. (1994). The role of fins in the competition between squid and fish. In *Mechanisms and Physiology of Animal Swimming*. Eds. Maddock, L., Bone, Q. and Rayner, J.M.V. pp. 27-43.

Houghton, E. L. and Carpenter, P. W. (1993). *Aerodynamics for Engineering Students*. New York: Halsted Press. pp. 460-486.

Jiang, H. and Grosenbaugh, M. A. (2002). Numerical simulation of vortex ring formation in the presence of background flow: Implications for squid propulsion. *Bull. Am. Phys. Soc*. **47**, 96.

Johnson, W., Soden, P. D. and Trueman, E. R. (1972). A study in jet propulsion: an analysis of the motion of the squid, *Loligo vulgaris*. *J. Exp. Biol.* **56**, 155-165.

Krueger, P. S. and Gharib, M. (2003). The significance of vortex ring formation to the impulse and thrust of a starting jet. *Phys. Fluids* **15**, 1271-1281.

Krueger, P. S., Dabiri, J. O. and Gharib, M. (2002). The effect of uniform background flow on vortex ring formation and pinch-off. *Bull. Am. Phys. Soc.* **47**, 95.

Krueger, P. S., Dabiri, J. O. and Gharib, M. (2003). Vortex ring pinchoff in the presence of simultaneously initiated uniform background co-flow. *Phys. Fluids* **15**, L49-L52.

Lighthill, M. J. (1969). Hydromechanics of aquatic animal propulsion—A survey. *Ann. Rev. Fluid. Mech.* **1**, 413-446.

Linden, P. F. and Turner, J. S. (2001). The formation of 'optimal' vortex rings and the efficiency of propulsion devices. *J. Fluid Mech.* **427**, 61-72.

McKenna, S. P. and McGillis, W. R. (2002). Performance of fundamental image velocimetry techniques. *Exp. Fluids*. **32**, 106–115.

Nauen, J. C., and Lauder, G. V. (2002). Hydrodynamics of caudal fin locomotion by chub mackerel, *Scomber japonicus* (Scombridae). *J. Exp. Biol.* **205**, 1709-1724.

O'Dor, R. K. (1988). Forces acting on swimming squid. *J. Exp. Biol.* **137**, 421-442.

Packard, A. (1969). Jet propulsion and the giant fibre response of *Loligo*. *Nature.* **221**, 875-877.

Pai, S. (1954). *Fluid Dynamics of Jets*. New York: D. Van Nostrand Company, Inc.

Prandtl, L. (1952). *Essentials of Fluid Dynamics*. London: Blackie and Son, Ltd.

Prandtl, L. and Tietjens, O. G. (1934). *Applied Hydro- and Aeromechanics*. New York: Dover Publications, Inc.

Rayner, J. M. V. (1979). A vortex theory of animal flight. Part 1. The vortex wake of a hovering animal. *J. Fluid Mech.* **91**, 697-730.

Rayner, J. M. V. (1988). Form and function in avian flight. *Curr. Orn.* **5**, 1-77.

Rayner, J. M. V. (1995). Wake vortex dynamics in swimming and flying vertebrates. In *Biological Fluid Dynamics* (ed. T. J. Pedley and C. P. Ellington). *Symp. Soc. Exp. Biol*. **49**, 131-155.

Schlichting, H. (1979). *Boundary Layer Theory*. New York: McGraw Hill.

Siekmann, J. (1963). On a pulsating jet from the end of a tube, with application to the propulsion of certain aquatic animals. *J. Fluid Mech.* **15**, 399-418.

Spedding, G. R., Rayner, J. M. V. and Pennycuick, C. J. (1984). Momentum and energy in the wake of a pigeon (*Columbia livia*) in slow flight. *J. Exp. Biol.* **111**, 81-102.

Streeter, V. L. and Wylie, E. B. (1985). *Fluid Mechanics, 8th ed*. New York: McGraw-Hill.

Trueman, E. R. and Packard, A. (1968). Motor performances of some cephalopods. *J. Exp. Biol.* **49**, 495-507.

Van Dyke, M. (1982). *An Album of Fluid Motion*. Stanford: The Parabolic Press.

Weihs, D. (1977). Periodic jet propulsion of aquatic creatures. *Fortschr. Zool.* **24**, 171-175.

Willert, C. E. and Gharib, M. (1991). Digital particle imaging velocimetry. *Exp. Fluids* **10**, 181-193.

Williamson, G. R. (1965). Underwater observations of the squid *Illex illecebrosus* Lesueur in Newfoundland waters. *Can. Field Natur*. **79**, 239-247.

Yamashita, H., Kushida, G., and Takeno, T. (1996). An experimental study on transition and mixing processes in a coaxial jet. In *Atlas of Visualization*, Volume II (ed. Y. Nakayama and Y. Tanida), pp. 53-66. New York: CRC Press.

Zuev, G.V. (1963). On the specific gravity of the squid *Ommastrephes sagittatus* Lamarck. trans. Foreign Languages Division, Department of the Secretary of State of Canada. Fisheries Research Board of Canada, translation series no. 998, from *Trudy Sevastopol'skoi Biologicheskoi Stantsii.* **16**, 383-386.

Zuev, G.V. (1965). The cephalopod body as an airfoil. Trans. US Department of Commerce. *Nauchnyye Doklady Vysshey Shkoly, Biologicheskiye Nauki. University Scientific Reports, Biological Sciences* **1**, 22-25.